Summer 2018

Application of Nano-Plasmonics for SERS Bio-Detection and Photocatalysis in the Same Platform

Muhammad R. Shattique
Missouri State University, sha22@live.missouristate.edu

APPLICATION OF NANO-PLASMONICS FOR SERS BIO-

DETECTION AND PHOTOCATALYSIS IN THE SAME PLATFORM

A Masters Thesis

Presented to

The Graduate College of

Missouri State University

In Partial Fulfillment

Of the Requirements for the Degree

Master of Science, Materials Science

By

Muhammad Rubaiet Shattique

August 2018

APPLICATION OF NANO-PLASMONICS FOR SERS BIO-DETECTION AND PHOTOCATALYSIS IN THE SAME PLATFORM

Physics, Astronomy and Materials Science

Missouri State University, August 2018

Master of Science

Muhammad Rubaiet Shattique

ABSTRACT

Nano-biological systems interfacing nano-structured solid surfaces with biological compounds such as oligonucleotides or proteins are highly regarded as enabling materials for biosensing and biocatalysis applications. In particular, nanostructures of noble metals such as gold or silver, when exposed to light, exhibit a phenomenon known as surface plasmon resonance. When a proper metal nanostructure (plasmonic substrate) is exposed to light, very efficient absorption of incoming photons is possible, resulting in a buildup of localized high-energy regions, or "hot-spots", where energetic carriers or "hot carriers" can be created. These hot-carriers can be used to catalyze desired chemical transformations in materials located nearby. Furthermore, plasmonic hot-spots are also known to enhance inelastic scattering of light by the same materials, promising multi-functional applications that combine photo-catalytic stimulation of materials with their ultrasensitive characterization in the same design. In this thesis work, we developed a conjugate nano-biological system interfacing plasmonic gold nanostructures with thiolated single-stranded DNA carrying an important reduction-oxidation indicator, methylthioninium chloride, also known as methylene blue. Using surface-enhanced Raman spectroscopy, we have detected characteristic bands of DNA-bound immobilized methylene blue in sub-monolayer quantities. We also have detected reversible reduction-oxidation of methylene blue during laser excitation of the samples at neutral pH, in the absence of electrodes or chemical agents.

KEYWORDS: nanoplasmonics, photocatalysis, SERS, nano-bioconjugates, hot-spots

This abstract is approved as to form and content

_____
Maria Stepanova, PhD
Chairperson, Advisory Committee
Missouri State University

APPLICATION OF NANO-PLASMONICS FOR SERS BIO-

DETECTION AND PHOTOCATALYSIS IN THE SAME PLATFORM

By

Muhammad Rubaiet Shattique

A Master's Thesis
Submitted to the Graduate College
Of Missouri State University
In Partial Fulfillment of the Requirements
For the Degree of Master of Science, Materials Science

August, 2018

Approved:

_____
Maria Stepanova, PhD

_____
Kartik C. Ghosh, PhD

_____
Keiichi Yoshimatsu, PhD

_____
Julie Masterson, PhD: Dean, Graduate College

ACKNOWLEDGEMENTS

TABLE OF CONTENTS

LIST OF FIGURES

CHAPTER ONE: INTRODUCTION

Light is our abundant source of energy. With growing population, increasing dearth of bio-mass based fuels and increasing environmental pollution due to greenhouse gases, light harvesting in order to store energy and using it subsequently has become a pressing demand of our time. Plasmonic nanostructures are very promising materials to harvest the energy of light. In particular, nanostructures of noble metals such as gold or silver, when exposed to light, exhibit a phenomenon known as surface plasmon resonance. Surface plasmons are oscillations of electron density at a surface of a metal. When a proper metal nanostructure (plasmonic substrate) is exposed to light, very efficient absorption of incoming photons is possible, resulting in a buildup of localized high-energy regions, or "hot-spots", where energetic carriers or "hot carriers" can be created. Energy of hot-spots may be used in a variety of ways, such as for example-inducing reduction-oxidation responses in biological materials. Furthermore, plasmonic hot-spots are also known to enhance inelastic Raman scattering of light by materials located nearby. The surface-enhanced Raman spectroscopy (SERS) allows capturing unique vibrational fingerprints of materials in sub-monolayer quantities, and as such it is highly regarded as a method of ultra-sensitive and selective bio detection. Combining energy harvesting from light, photo-catalytic stimulation of materials, and ultrasensitive SERS characterization of molecular events in the same design promises numerous transformative applications.

This research work is an experimental work, which demonstrates a multi-functional application of plasmonic nanostructures. In this research, we have devised a way of synthesizing plasmonic nano-structures in a simple way. Also, we have devised a way of bio functionalizing of these plasmonic substrates that is suitable for immobilizing molecules from solutions. We were able to immobilize a pigment known as Methylene Blue (MB) from a solution on our substrates. Then, we detected sub monolayer quantities of the pigment by Surface Enhaced Raman Spectroscopy (SERS) technique. Furthermore, we carried out chemical modification (reduction-oxidation) of the immobilized pigment on our palsmonic substrates by merely exposing them to laser light at neutral pH and without the application of electrode potential. We successfully monitored these chemical changes on the same system using SERS.

CHAPTER TWO: LITERATURE REVIEW

2.1 Nanoplasmonics

Metals are bonded through metallic bonding, which is a result of the electrostatic attractive forces between electrons and metal ions that eventually form bulk metals. In a metal, valence electrons are detached from metal ions, which form a periodic lattice. The valence electron are shared over the entire metal volume, such that the metal ions are immersed in a "sea" of mobile valence electrons. The strength of metallic bonding is related to the density of these delocalized electrons (Anker et al., 2008a). However, when the size of metals is less than the wavelength of light their properties also change. Usually, the electrons have a mean free path of 40nm-50nm in noble metals such as Gold (Au) (Bantz et al., 2011b). Nanoparticles of these noble metals can be synthesized with sizes less than 50 nm (Sylvia, Janni, Klein, & Spencer, 2000). When an electromagnetic (EM) wave such as light is incident on nanoparticles, it interacts with their surface. If the frequency of the incident photons is close to the plasma frequency of the free electrons on the surface of metal nanostructures, it will lead to a collective oscillation commonly known as the localized surface plasmon resonance (LSPR). (Barnes, Dereux, & Ebbesen, 2003; Homola, Yee, & Gauglitz, 1999). Surface plasmons are resonant oscillations of conduction electrons in nanoparticles exposed to light. The collective oscillation of electrons results to an enhancement of the local EM field, which is predominantly confined to the metal surface. Following the resonant excitation, the Plasmon decays within tens of femtoseconds. The decay can take place through radiative photon emission

(i.e., scattering) and/or through generation of energetic charge-carriers at the nanoparticle surface. These energetic electron–hole pairs are termed hot electrons/holes (Ye, Long, Huang, & Xiong, 2017). The shape and size of nanoparticles determine the electron density, which in turn determines plasmonic oscillations (Cheng, Mayes, & Ross, 2004). For example, the dielectric constant of environment can influence plasmonic oscillations of electrons (Cheng et al., 2004).

When two closely positioned metal nano-particles are exposed to light, a localized electromagnetic field is formed between and around the nanoparticles. This localized EM field is termed as 'Hot spots' in the field of nano-plasmonics (Cheng et al., 2004). Thus synthesis of nanostructures that can maximize the hotspot generation has been addressed extensively in the recent years (Xie & Schlücker, 2014). The plasmonic substrates can be fabricated through vapor synthesis techniques such as thermal evaporation, or magnetronic sputtering of noble metals on glass substrates. The roughness of the deposited metal and the close proximity between neighbor crystallites are often sufficient to generate hotspots. Due to randomness of such structure, control over size and location of hotspots is limited. Compared to such easy to use but difficult to control techniques, nanolithography presents the opportunity of a greater control over nanostructures (Dieringer et al., 2006) . Nano-sphere lithography (Giljohann et al., 2010; Li et al., 2018) and electron beam lithography (Peters, Gutierrez-Rivera, Dew, & Stepanova, 2015) are the most common lithographical techniques used to produce plasmonic nanostructures. Other methods used to create controlled nanostructures include block co polymer template synthesis (Peters et al., 2015) and selective etching of bimetallic nanoparticles (Peters et al., 2015). Another promising way to produce plasmonic substrates is by self-

assembly of colloidal nanoparticles. The key in success of this method is to functionalize

nanoparticles in a way that can tune their aggregation propensity (Peters et al., 2015). For

example, DNA functionalization of nanoparticles to create tunable nanostructures that

can generate plasmonic hotspots have been vigorously researched and very successful

(Cao, Jin, & Mirkin, 2002b; Mirkin, Letsinger, Mucic, & Storhoff, 1996).

2.2 Raman Scattering of Light

Sir C. V. Raman and K.S. Krishnan together discovered that the light can scatter

from materials with a change in frequency (Raman & Krishnan, 1928) (Fig.2.1). The

shifts in frequency depend upon the molecules light interacts with. The differences in

wave number between the incident radiation and the scattered light are related to

vibrational and rotational energy states of the molecules. In contrast, elastic scattering of

radiation by matter occurs without frequency shift. Known for a long time as the

"Rayleigh" or "Tyndall" scattering, elastic scattering explains, for example, the blue color

of the sky. However, the "Raman effect" has been discovered significantly later because

of the low probability of its occurrence during interactions between photons and

molecules. Only one in $10^6 – 10^{10}$ photons would undergo inelastic scattering (Raman &

Krishnan, 1928).

In Raman Effect the interaction is not a simple act of fluorescence. During

fluorescence a molecule absorbs a photon, and another one of different frequency is

emitted. In that case, the incoming radiation is actually absorbed by the molecule. In

contrast, in the Raman Effect such an absorption is not necessary.

The Raman Effect is utilized in the spectroscopy technique called the Raman spectroscopy, which is a very useful and versatile non-destructive characterization technique. Raman spectra are representative of vibrational characteristics of a material. Since Raman spectroscopy can detect various modes of molecular vibrations, it captures unique vibrational fingerprints of many materials including crystalline solids, non-crystalline solids, biological species, liquids, thin films, etc.
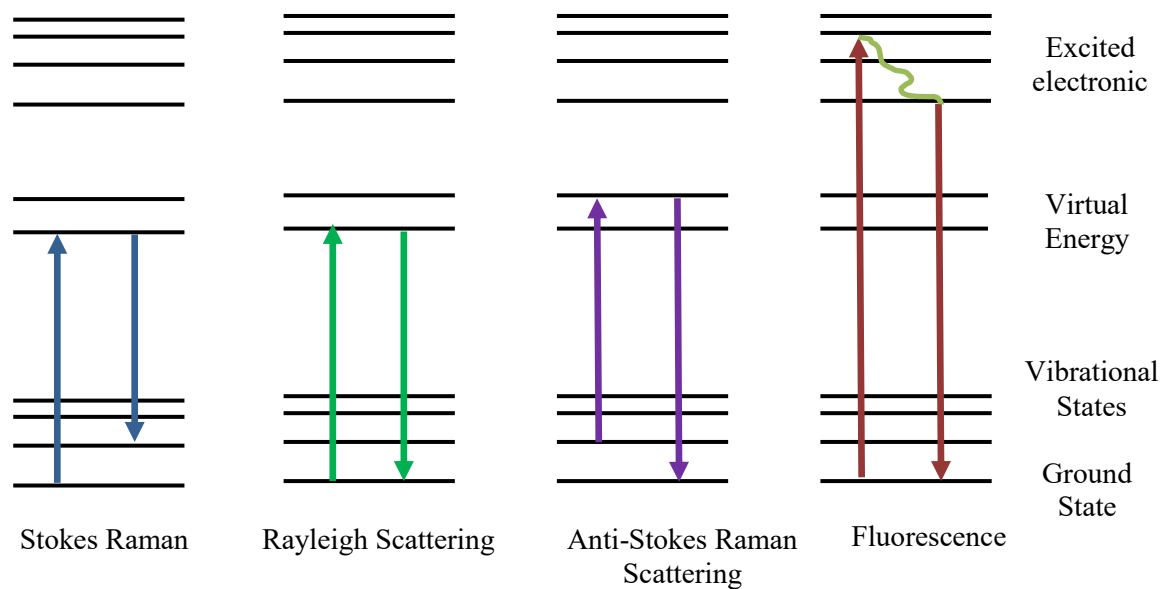
Fig. 2.1. Schematic Energy diagram explaining the Raman effect (Haynes, McFarland, & Duyne, 2005)

A simplified setup of Raman Spectroscopy consists of monochromatic filter (excitation filter) which allows only light with a specific wavelength to reach the sample. The measured scattered light exhibits a broader spectrum of wavelengths. A second filter (emission filter) behind the sample allows blocking of the incident wavelength. This allows to separate observed scattered light from the incident light (Fig. 2.2).

6

The light source of a Raman spectrometer is in general a laser with a specific wavelength. The laser's wavelength typically ranges from 400 nm to 800 nm depending on the application. In Raman spectra, the intensity of measured Raman scattering is plotted versus the frequency shift. The Raman frequency shift is defined as a difference between the measured frequency of scattered light and incident light. Therefore, Raman spectra are independent of the wavelength of the light source. However, instead of using the wavelength, the Raman shift is conventionally given as change of the wavenumber (cm^{-1}) which is inversely proportional to the wavelength. The intensity of scattered light is plotted against the wavenumber in a typical Raman spectrum. For example, Fig. 2.3. shows a Raman Spectrum of water on a Si substarte. The intensity of scattered light is plotted as a function of a shift in frequency here. Characteristic Raman bands of water ($3200\ cm^{-1}$-$3500\ cm^{-1}$) and silicon ($530\ cm^{-1}$) are clearly seen in this plot.
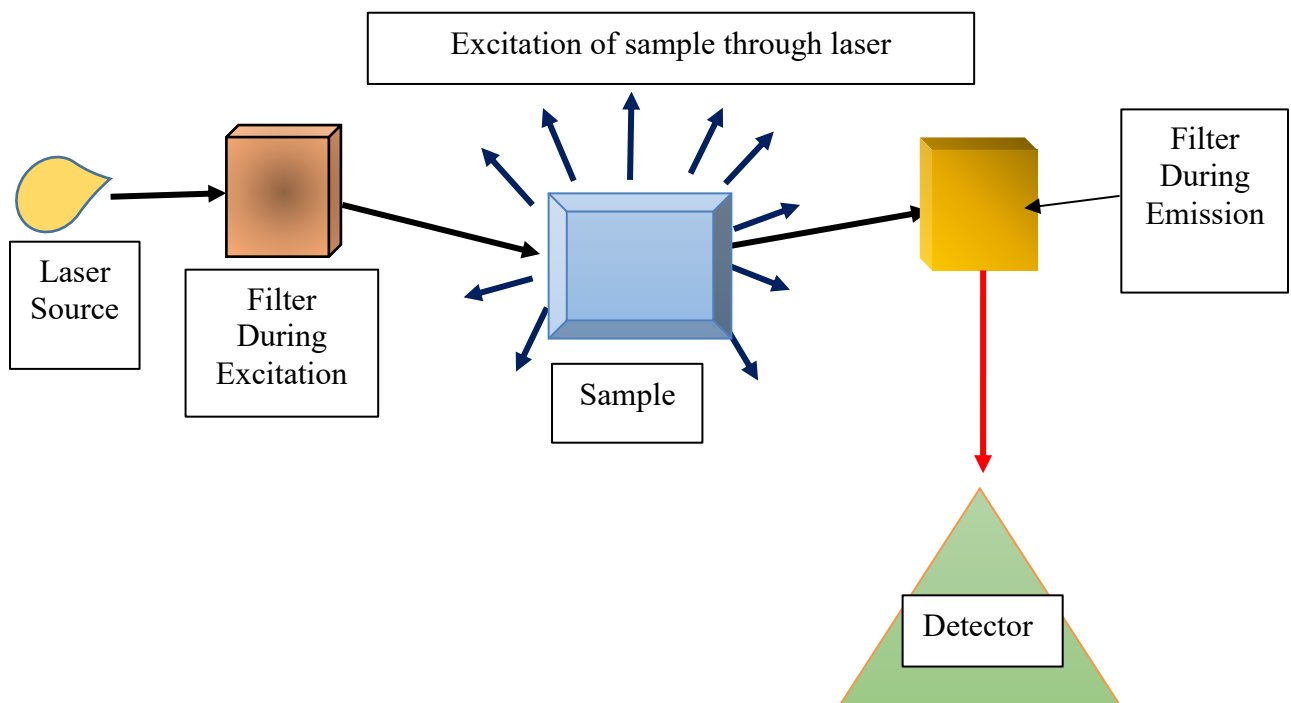
Fig. 2.2. Schematic diagram of a Raman experiment setup (Knight & White, 1989)
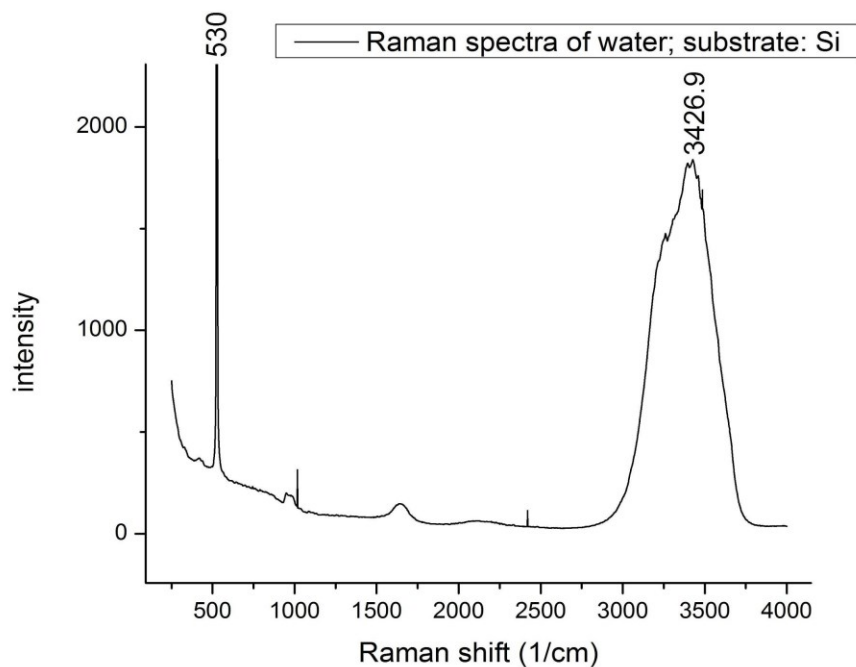
Fig. 2.3. Typical Raman Spectrum of water on a silicon substrate.

2.3 Surface Enhanced Raman Spectroscopy (SERS)

The Raman scattering is enhanced by the presence of plasmonic nanostructures (Haynes et al., 2005) (Fig. 2.4.). Hot-spots generated by these nanostructures interact with the Raman scattering, and this interaction results in a 10^3-10^6 times enhancement of the inelastic scattering (Sharma, Frontiera, Henry, Ringe, & Van Duyne, 2012; Zeng, Liu, & Wei, 2016). The origin of this enhancement effect is still debatable. Two models have been proposed to explain Surface-Enhanced Raman Scattering (SERS), Chemical enhancement and Electromagnetic field enhancement (Sharma et al., 2012). According to the chemical enhancement model, the nature of the molecules that interact with light

determines the enhancement factor. Different chemical environment around the same molecule will produce a different enhancement effect depending on its chemical composition. The localized EM field in the hot spots plays a key role in the enhancement of the Raman Effect according to the electromagnetic field enhancement model. The size, shape and interparticle distance can influence the localized EM field strength, thus influencing the overall scattering enhancement (Zeng et al., 2016).
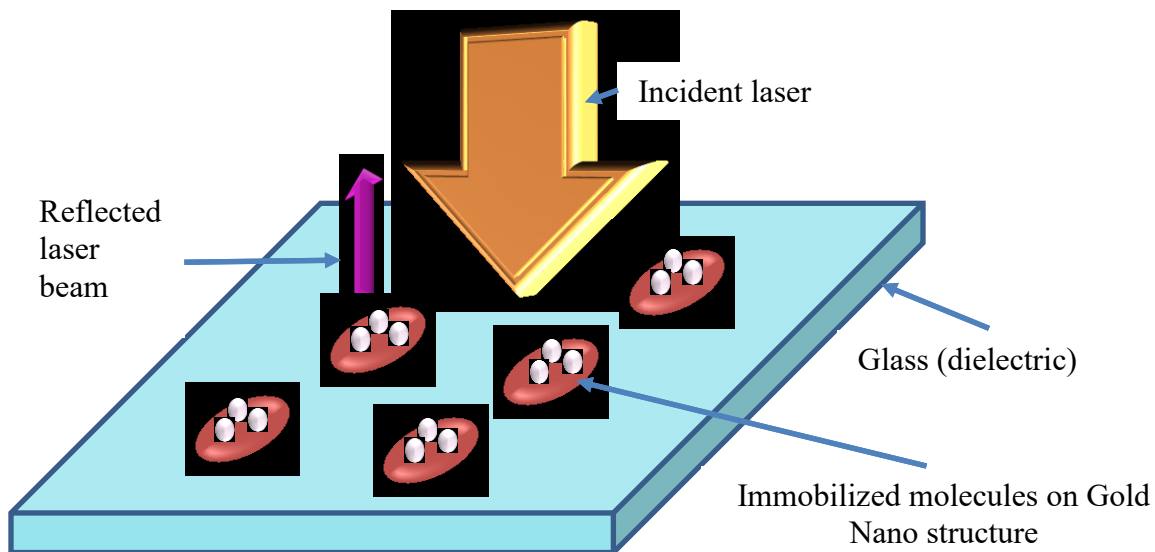
Fig. 2.4. A schematic diagram of SERS arrangement. (Peters et al., 2015)

2.4 Applications of SERS

For regular Raman spectroscopies, a large number of molecules are required to generate enough scattered photons to be detected. For example, if one uses a 100mW laser with a 1 μm of laser focus area, a single molecule will emit only 10^4 photons per

second. This is a very small amount, which will in turn make the experimentalist to wait more than an hour to detect a single scattered photon. SERS enhances the photon signal significantly amount, which enables the observer to detect Raman photons coming from a single molecule more easily (H. Liu et al., 2011). This effect has been instrumental for fingerprint detection from monolayers of molecules (Ravindran, Chandran, & Khan, 2013). Detection of nano-sized biological entities such as DNA, and even identification of individual bases Adenine, Guanine, Cytosine, or Thymine was accomplished using SERS (Cao, Jin, & Mirkin, 2002a). Moreover, living entities such as living cells can be detected using SERS too (Cao et al., 2002a). This means that plasmonic nanostructures that utilize SERS can be effective biosensors (Bantz et al., 2011a). This paves the way of in vivo spectroscopy of living organisms. Besides, SERS has been utilized to detect chemical warfare agents. With the development of portable Raman spectroscopes, this technique can be used for the security purposes (Brosseau, Casadio, & Van Duyne, 2011). SERS can be used in electrochemistry also. Many chemicals change their oxidation states with the change of potentials, and these oxidation states can be detected through SERS because different oxidation states has different vibrational frequencies (Oakley, Dinehart, Svoboda, & Wustholz, 2011). Chemical present in a very small amount is of huge interest in preserving old art pieces and detecting imitations. SERS has been used in this field extensively (Roh, Matecki, Svoboda, & Wustholz, 2016). SERS is also used in ultrafast and femtosecond spectroscopy with the idea that noble metal nanostructures that enhance the Raman signals also allow to detect charge transfer mechanisms in molecules precisely (Paxton, Kleinman, Basuray, Stoddart, & Van Duyne, 2011). In nano-bioconjugates plasmonic nanostructures are functionalized by a biological

entity. So far, these nanobioconjugates sensors have been used for DNA/Aptamer based sensing, protein/enzyme/peptide/antibody SERS biosensing, cellular and in vivo sensing (Weitz, Garoff, Gersten, & Nitzan, 1983). One can extract both qualitative and quantitative information from the SERS spectra.

2.5 Multifunctional Applications of Nano-plasmonics

Free electrons on the metal surface can have strong interactions with incident photons as discussed in section 2.1. Surface plasmon resonance is a powerful tool to concentrate light at the metal–dielectric interface. Thus, plasmonic metal nanostructures offer high capabilities for light trapping and electromagnetic field enhancement. The surface plasmon resonance has potential applications in photo catalysis (Ye et al., 2017) and photovoltaics (Kulkarni, Noone, Munechika, Guyer, & Ginger, 2010) and sensing (Anker et al., 2008b) as well as in surface-enhanced Raman scattering (SERS) as discussed in previous section

In a photo-catalysis process solar energy is converted to chemical energy. This energy is usually stored in chemical bonds of molecules. In a typical photocatalytic process, light of appropriate energy is absorbed. This absorbed energy excites the electrons, which in turn generates photo-excited electrons and holes. The photo-generated electron–hole pairs are then separated and transferred to the surface. These electron–hole pairs take part in reduction-oxidation reactions. The photocatalytic effects of nano plasmonics can be used in water splitting, carbon di-oxide reduction, degradation of organic pollutants etc. (Ye et al., 2017). Plasmon-assisted photo catalysis is very promising as it selectively oxidizes organic substrates. Traditional catalytic oxidation

processes usually occur under high temperature, pressure and/or extreme pH conditions. In the case of nano-plasmonics- the hot carriers that are generated, may influence the oxidation mechanism by favoring the adsorption of intermediate species and/or of oxidizing agents. This significantly improves selectivity of the reaction. (Kim, Lee, Moon, & Park, 2016a)

Hot electrons at the metal surface are generated in several steps (Kim et al., 2016a). First, the metallic nanostructure is excited using light; this light has a much larger wavelengths than the size of metal nanoparticles. Next, the excited charges can decay either radiatively into a photon (scattering) or nonradiatively into hot carriers. Non radiative decay is considered as an effective pathway for generating hot electrons at the metal surface. Eventually, these hot electrons transfer their energy into specific electronic states of molecules that are adsorbed on the metal surface through many different ways (Persson & Ryberg, 1981). This phenomenon may take place prior to losing the energy of hot-electros by either electron–electron scattering or electron– phonon coupling at a femtosecond to picosecond time scale (Fig. 2.5.) (Kim, Lee, Moon, & Park, 2016b) .

Plasmon driven photo-catalysis can occur through thermal pathways or directly by hot-carriers (Kim et al., 2016b). A large number of reactions such as ammonia synthesis, hydrocarbon reforming, oxidation and hydrogenation reactions are thermally activated processes that can be thermally catalyzed using metal NPs. Thermal catalysis on metallic surface is primarily a process which is phonon-driven. Decay of hot electrons can activate phonon modes of the metal.
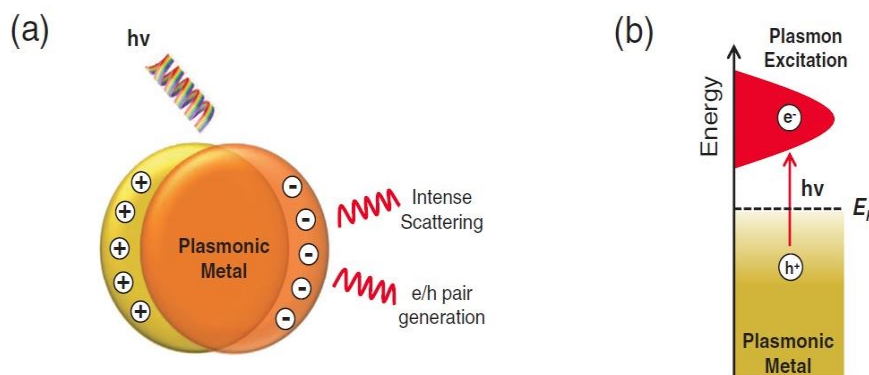
Fig. 2.5. (a) Schematic and (b) energy diagram showing the generation process of plasmonic hot carriers by light-induced excitation of SPR on a metal nanoparticle. Reproduced with permission from Ref (Kim et al., 2016b).

Then absorbed molecules' vibrational modes couple with the phonon modes of the metal. In such case, different thermal activation pathways are possible. This usually results in a large number of unwanted bi-products, In contrast, direct plasmonic photocatalysis tends promoting selective chemical reactions thus overcoming limitations of thermal catalysis (Kim et al., 2016b). Plasmon-induced heating can be insignifant under low intensity exposures. Hot carriers can be transferred to adsorbate molecules through some kind of charge transfer. These reactions may include hot carriers injection to the molecular orbital of a targeted molecule followed by coupling between plasmonic strucutres' excited electronic state and adsorbates. reaction pathways. (Fig. 2.6). In this way specific and sometimes otherwise inaccessible reaction pathways can be activated (Chen, Zhu, Zhao, Zheng, & Gao, 2008; Naldoni et al., 2016).

Nanoplasmonics also has promising applications in photovoltaics (PVs) especially when used in conjuction with the conventional photovoltaic cells. The application is similar to the photocatalytic process in a way that it also requires hot carrier generation and carrier transfer. Conventional PV thin films are suffering efficiency issues due to

rapid recombination of electron/ hole pairs and high reflectance i.e poor absorption of light.

Also, many semiconductors have bandgap in the UV region, which make them unsuitable for almost 70-80% of solar spectrum absorbance which consists of visible to near infrared light. Plasmonic nanostructures can be very effective for *light trapping*, which will increase the light absorption of PVs (Atwater & Polman, 2010).

Additionally, hot carriers generated by plasmonic nanostructures can be transferred to the conduction band of semiconductors, which can increase the efficiency of the PVs (D. Liu et al., 2016; Wu, Chen, McBride, & Lian, 2015) . The electromagnetic enhancement in the LSPRs can increase the photocurrent of the PV's also (Dey & Zhao, 2016) (Fig. 2.7).
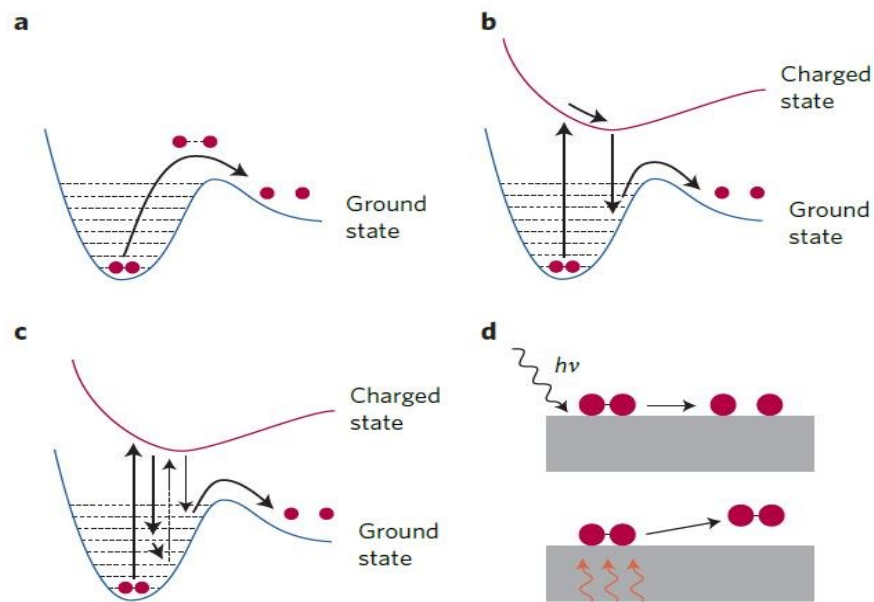
Fig. 2.6. (a) Di-atomic molecules are dissociated through thermal activation. (b) The dissociation of di-atomic molecules with the help of electrons. (c) When the incident flux of photon is high, electron can get injected in the di-atomic molecule before the molecular vibration is dissipated completely. (d) Plasmonic metal nanoparticles induce electron-driven reactions (top), which can trigger certain chemical reaction pathways that are not accessible otherwise (bottom). Reproduced with permission of Ref (Atwater & Polman, 2010).
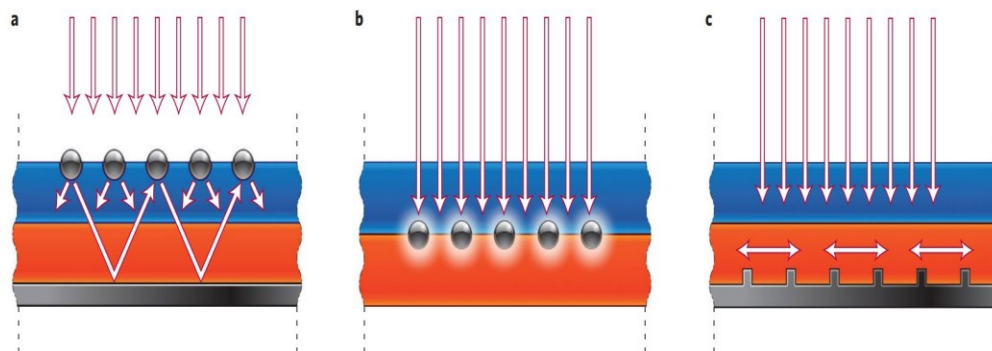
Fig. 2.7. Plasmonic light-trapping geometries for thin-film solar cells. (a) Light is trapped through scattering from metal nanoparticles at the surface of the solar cell. (b) Light can be trapped when it excites localized surface plasmons in metal nanoparticles embedded within the semiconductor. (c) When the excitation of surface plasmon polaritons occurs at the metal/semiconductor interface, light also is trapped. Reproduced with permission from Ref (Naldoni et al., 2016).

15

CHAPTER THREE: OBJECTIVES

Importantly, the various functionalities of nanoplasmonics can be combined in a single platform. In this work, we attempted to induce chemical changes (reduction-oxidation) to a pigment, methylthioninium chloride or Methylene Blue (MB) by using nano-plasmonics, and to detect these changes by SERS in the same platform. The premier objectives of this work are as follows:

- Preparing and optimizing of Au coated nano- plasmonic substrates.
- Bio-funtionalizing of plasmonic substrates and immobilizing MB pigment from solution.
- Inducing chemical changes (reduction-oxidation) of immobilized MB pigment through plasmonic hot-spots, and detecting these changes by SERS in the same sample.

CHAPTER FOUR: METHODS

In this section methods used in substrate preparation, bio-functionalization and characterization will be discussed.

4.1 Instruments Used for Plasmonic Substrtate Fabrication and Characterization

The plasmonic substrates consist of noble metal nanostructures on dielectric supports because this enhances the surface plasmon resonance effect. Sputtering by ion bombardment is a very useful way to prepare metal nanostructures, as this is easy and effective. In the basic sputtering process, a target (or cathode) is bombarded by high-energy ions. The bombardment causes the removal of target atoms. These atoms fly in a vacuumed chamber, resulting in a thin film deposited on a substrate.(Kelly & Arnell, 2000) A broadly used version of this process is known as magnetron sputtering. Magnetrons employ electric field configured such that ions from a plasma are directed towards a surface, whereas secondary electron motion is confined in the vicinity of the target. As a result the probability of ionization of a gas in the chamber through electrom-atom collisions substantially increase, producing a dense plasma, which results in an incresead bombardment at the target. This is turn results in a faster sputtering and, therefore, the rate of deposition at the substrate is high (Thornton, 1978). In our research, we used an Emitech K550X sputter coater from Quoram Technologies situated at Jordan Valley Innovation Center (JVIC). (Fig. 4.1.) It has the following features:

- Fully Automatic Control
- Low Voltage Sputtering

- High Resolution Fine Coating (Order of 2nm Gold Grain)

Fig. 4.1. Emitech K550X sputter coater from Quoram Technologies (Adapted with permission from Quoram Technologies).

Specification of Emitech K550X:

- Instrument Case 450mm Wide x 350mm Deep x 175mm High

- Work Chamber Borosilicate Glass 165mm Dia x 125mm High

- Safety Shield Polycarbonate

- Weight 18 Kg

- Target 60mm Dia x 0.1mm Thick (Gold fitted as Standard)

- Specimen Stage 60mm Dia. Rotating Stage with Tilt facility. (Spacing to

- Target 40mm)

- Vacuum Gauge Range ATM - 1x10-4 mbar

- Deposition Range 0-50mA

- Deposition Rate 0-25nm/Minute

- Sputter Timer 0-4 minutes

- Pre-set Needle Valve Control of Argon Supply

The atomic force microscope (AFM) system is a useful tool for direct measurements of micro-structural parameters and determining the intermolecular forces at nanoscale level with nanometric-resolution precision. Typically, AFM works on three modes; non-contact mode, contact mode, and tapping mode. The non-contact mode is utilized by moving the cantilever slightly away from the sample surface and oscillating the cantilever at or near its natural resonance frequency. It can probe electric, magnetic, and/or atomic forces of a selected sample. The contact mode acquires sample attributes by monitoring interaction forces while the cantilever tip remains in contact with the target sample. The tapping mode of operation combines qualities of both the contact and non-contact modes by gleaning sample data and oscillating the cantilever tip at or near its natural resonance frequency while allowing the cantilever tip to impact the target sample for a minimal amount of time.(Jalili & Laxminarayana, 2004; Meyer, 1992) In our research we have used a Bruker Dimension Icon AFM instrument of the Jordan Valley Innovation Center (JVIC). The instrument is equipped with a Nanoscope V controller, and operates in a tapping mode.

For cleaning of glass substrates, we used a sonicator and a plasma etcher. During sonication, the energy of sound waves is applied to clean the substrate. Usually ultrasonic (>20 KHz) sound frequencies are applied. These waves migrate through a medium

inducing pressure variations which in turn transforms the sound waves into mechanical energy. (Doktycz & Suslick, 1990) In our research we used a Bransonic 0.5 Gallon Ultrasonicator for substrate cleaning purposes. (Fig. 4.2.)

Fig. 4.2. Sonication bath.

We also used plasma etching to make sure there is no unwanted species on our substrate (Fig 4.3.). Plasma etching process uses a dense plasma consisting of electrons, ions, free radicals and molecules which constantly bombard the substrate. Depending on the gases that are used in forming the plasma, one can achieve both mechanical and

chemical cleaning.(Doktycz & Suslick, 1990) We used a RF plasma etcher of Jupiter III (Nordson March) instrument at JVIC with help of Rishi Patel to plasma etch our substrates.

Fig. 4.3. Plasma Etcher.

The Raman characterization was carried out with a Horiba LabRAM HR 800 Evolution Raman spectroscope. A 532 nm green laser was used for the Raman excitation, and the Stokes scattering was received with edge filter and detected by a CCD detector. The Edge filter blocks out and filters elastic Rayleigh scattering. The Band-pass filters

that are used in Raman pass only certain wavelengths and absorbs all other wavelengths. In this research, edge filter is used. Edge filters only let the Stokes scattered photons to pass. (Fig. 4.4).

The characterization parameters were optimized for Raman characterization of liquid samples. We used a 10X microscope lens for our focusing purpose of the samples (Fig. 4.5 and Fig. 4.6.). The photons that were able to make it through the edge filters (i.e. photons having larger wavelengths than the incident light) were passed through a 300µm confocal hole.
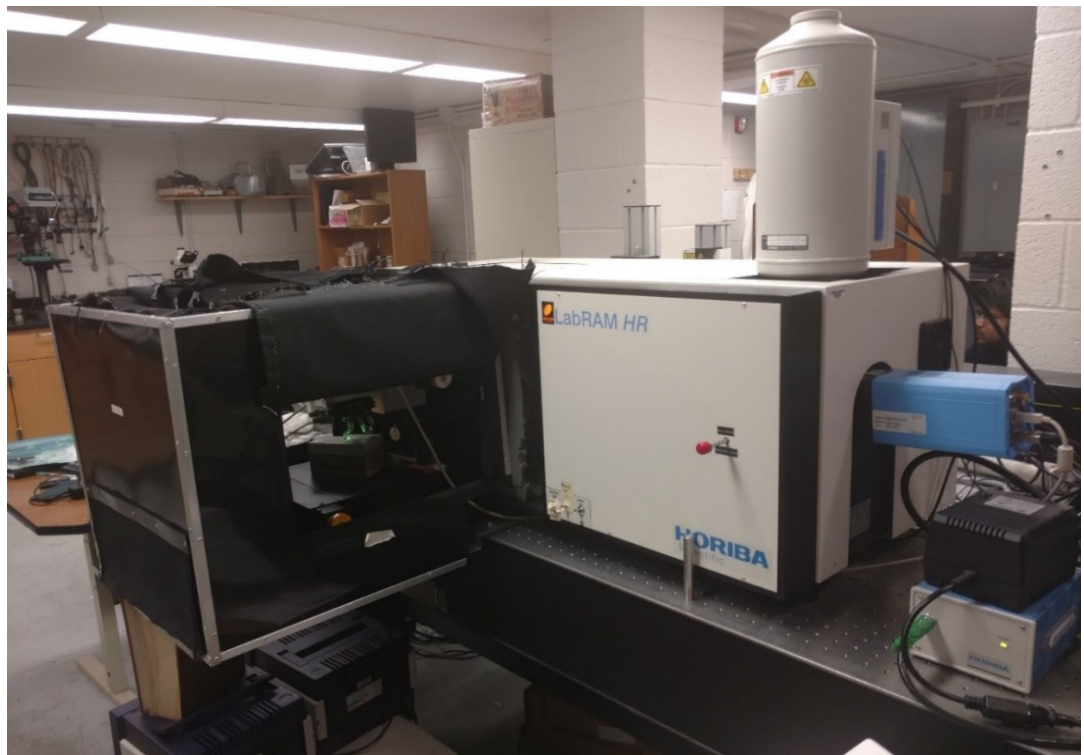
Fig. 4.4. Horiba LabRAM HR 800 Evolution Raman spectrometer
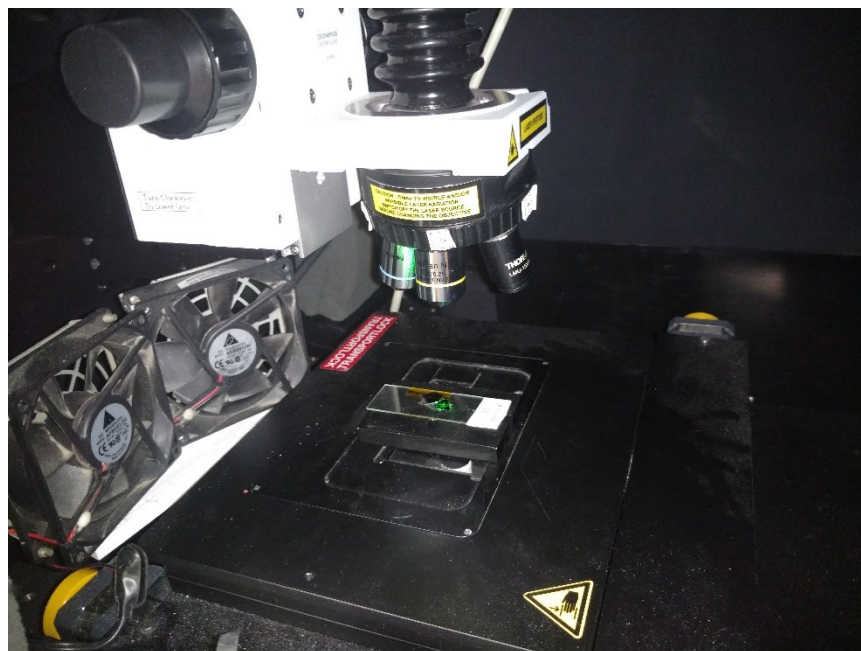
Fig. 4.5. Raman spectroscopy setup: A 10x microscope is exposing 532 nm laser on a substarte.
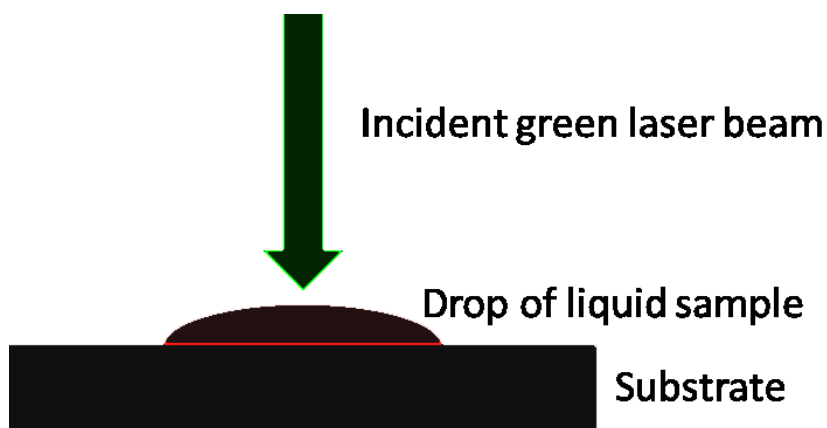
Fig. 4.6. Schematic of the experimental setup of Raman spectroscopy of liquid Samples.

We used a Laser Quantum Torus 532nm Green laser with a mpc3000 power source with 50mW laser power as our laser source Fig 4.7. The detailed specifications of the Torus laser are listed below:

Wavelength	532 nm
Beam Size	1.7 mm ± 0.2mm
Bandwidth	1 MHz
Power stability	< 1.0% RMS
RMS noise	< 0.5%
Noise bandwidth	1Hz - 100MHz
Coherence length	> 100m
Operating temperature	15 - 35° C
Head weight	1.2 kg
Warm-up time	<30 mins

Fig. 4.7. Taurus mpc300 532nm Green lase by Laser Quantum.

NGS LabSpec 5 software was used to display and store the data. To analyze the

Raman spectra, background subtraction was done by the OriginPro 8.5.1 software. Prior

to this Raman data were saved as a .txt file using LabSpec 5. Backgroud subtraction was

performed using a 4th order polynomial interpolation. The Raman spectrometer was

calibrated by using a standard silicon wafer regularly.

4.2 Instruments and Chemicals Used for Biofunctionalization

We used Tris-EDTA buffer solution from Sigma Aldrich. (Fig.4.8). It is a common buffer solution that is used to solubilize DNA and RNA without degrading them (Yagi et al., 1996).

Sulfur is attached to Au by chemisorption. DNA can be attached to Au surfaces by mediation of sulfur (thiol) groups (Pensa et al., 2012). The thiol-Au bond is very strong (40/50 kcal/mole). We purchased lyophilized thiolated single stranded DNAs 5'-GGTTTGGAGGGGC CA-3' from Sigma Aldrich for bio-funtionalization of our Au coated glass substrates.(Pensa et al., 2012)

A pH meter is employed to measure the alkalinity and basicity of a solution. In this research we used a calibrated standard pH meter to monitor the pH of Tris-EDTA buffer and DNA solutions. A Vortex mixer from Fisher Scientific was used to make the DNA solution. Micropipette was used to transfer the small amounts of solutions.

As our target analyte we used Methylthioninium Chloride popularly known as Methylene Blue (MB). Molecular formula of Methylene Blue is $C_{16}H_{18}ClN_3S$. Methylene Blue is a very common oxidation-reduction indicator. In its oxidized state it is blue in color and in reduced state it is colorless. This reduced state is known as Leucomethylene Blue and has a molecular formula $C_{16}H_{19}N_3S$ .We purchased a 1.5% solution of Methylene Blue from Sigma Aldrich for our research. We used HPLC grade water from Thermo Fisher to dilute some of the solutions. (Fig. 4.8).
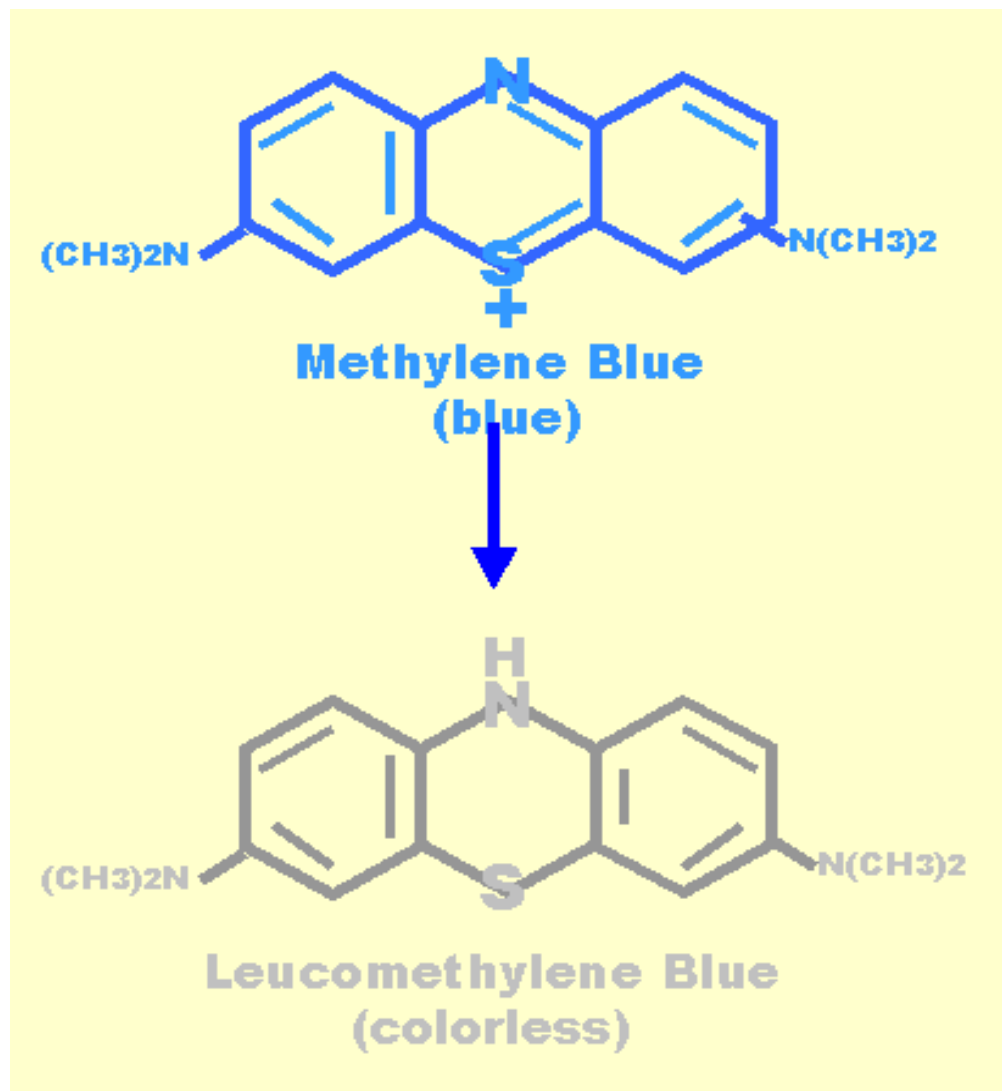
Fig. 4.8. Oxidized (top) and reduced (bottom) structures of methylene blue. Reproduced with permission from Ref. [50].

The solutions were preserved in test tubes purchased from Sigma Aldrich. The glass slides that we used for Au coated glass substrate were purchased from Thermo-Fisher Scientific. A medical grade refrigerator was used for the incubation purpose.

CHAPTER FIVE: RESULTS

5.1 Protocols Used to Fabricate Nano-Bio Conjugate System

Plasmonic nanostructures were created by magnetronic deposition of thin gold coating on glass substrates using a sputter system with a deposition rate of 10 nm/min. Prior to the Au coating, a thorough cleaning of glass substrates was done. The glass substrates were first washed with acetone and DI water; then they were taken to sonication bath for acetone sonication for 5 min. After the sonication, each sample was nitrogen-dried. Finally, the substrates were RF plasma-etched. Etching was performed for 1 min with a mixture of Ar and H2 followed by 30 sec of H_2 etching (Fig. 5.1.).

We have employed the Atomic Force Microscopy (AFM) to characterize our gold coated glass samples. The atomic force microscopy results show surface morphology and roughness of gold coated galss substartes at varying thickness of coating. (5nm, 10nm, 15nm, 20nm, 25nm & 30nm) (Fig. 5.2. & Fig.5.3.). From these figures we can observe that the sputter deposition of Au creates random islands of Au nano-structures. The surface area of an individual nano-structure increases with the increased deposition time. The distance between any two nanostructures decreases with increased deposition thickness. A 5nm thickness coating has the highest relative roughness followed by 10nm, 15nm, 20nm, 25nm and 30nm, which has the least relative roughness.

By comparing the results of roughness, nanostructure surface area and distance between adjacent nano-structures, we identified 15 nm as our desired thickness of Au coating on glass to function as our plasmonic nanostructure.

2% H$_2$SO$_4$ cleaning solution
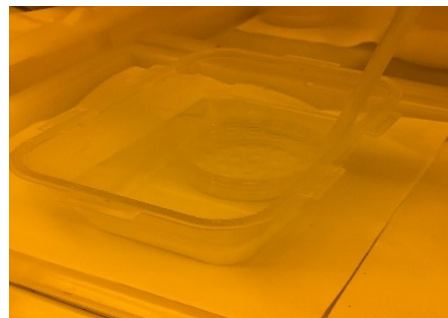
5 min dipping in cleaning solution
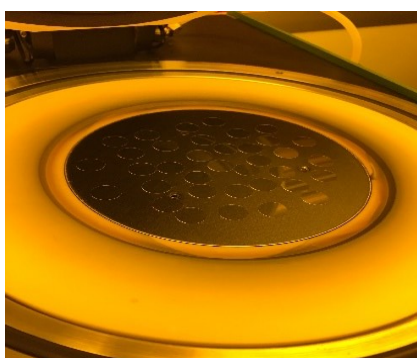
Clean slides placed on a plasma cleaning platform

Acetone sonication for 5 mins.

Sputtering carried out by fixing up parameters that ensures a 10 nm/min deposition

1 min Ar+O$_2$ plasma cleaning followed by a 30 sec Ar cleaning only

Fig. 5.1. Au coated glass substrate preparation steps.
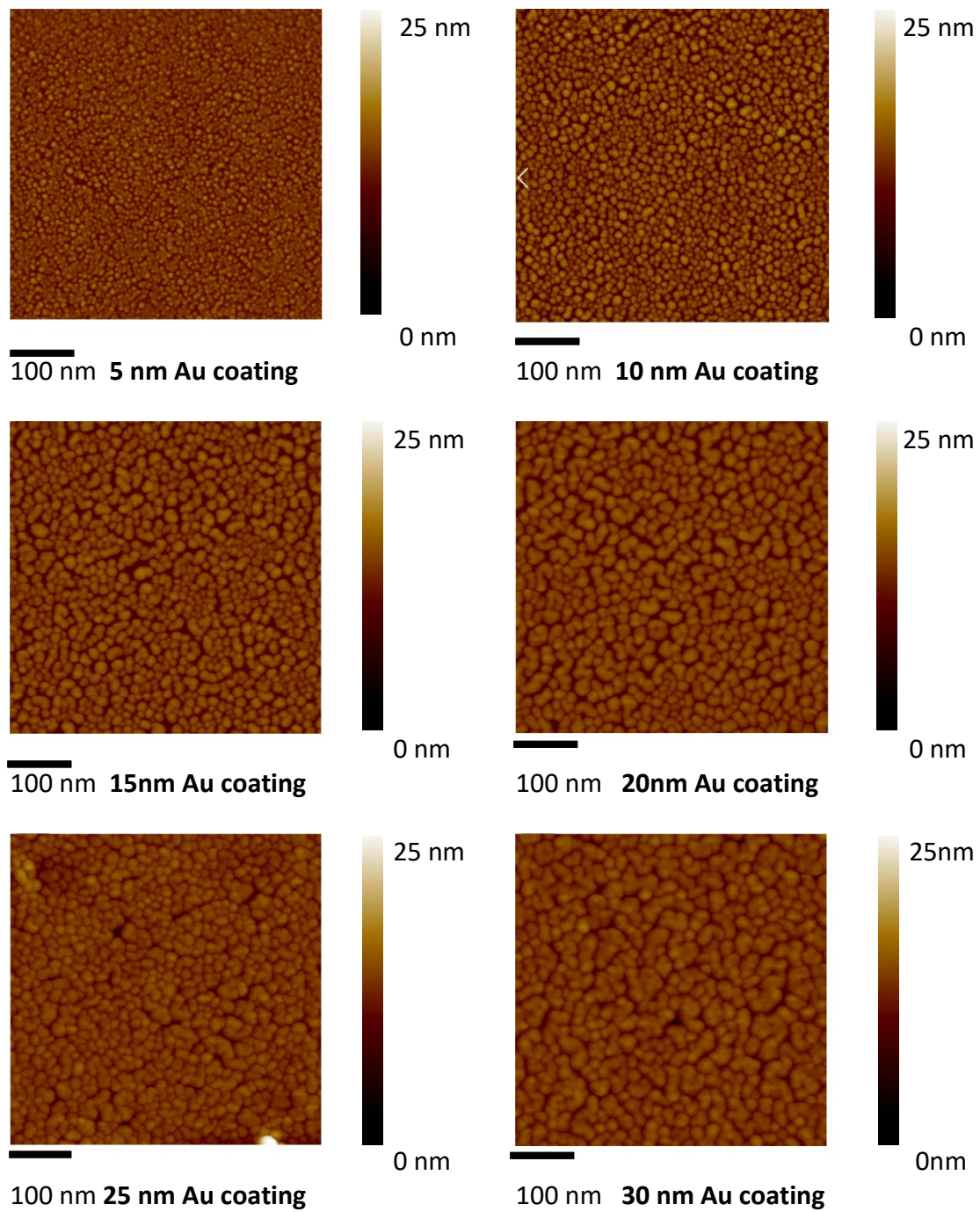
Fig. 5.2. AFM surface morphology of Au coated glass substrates at different coating thickness (5nm -30nm).

30 nm thickness of Au

25 nm thickness of Au

20 nm thickness of Au

15 nm thickness of Au

5 nm thickness of Au coating

10 nm thickness of Au coating
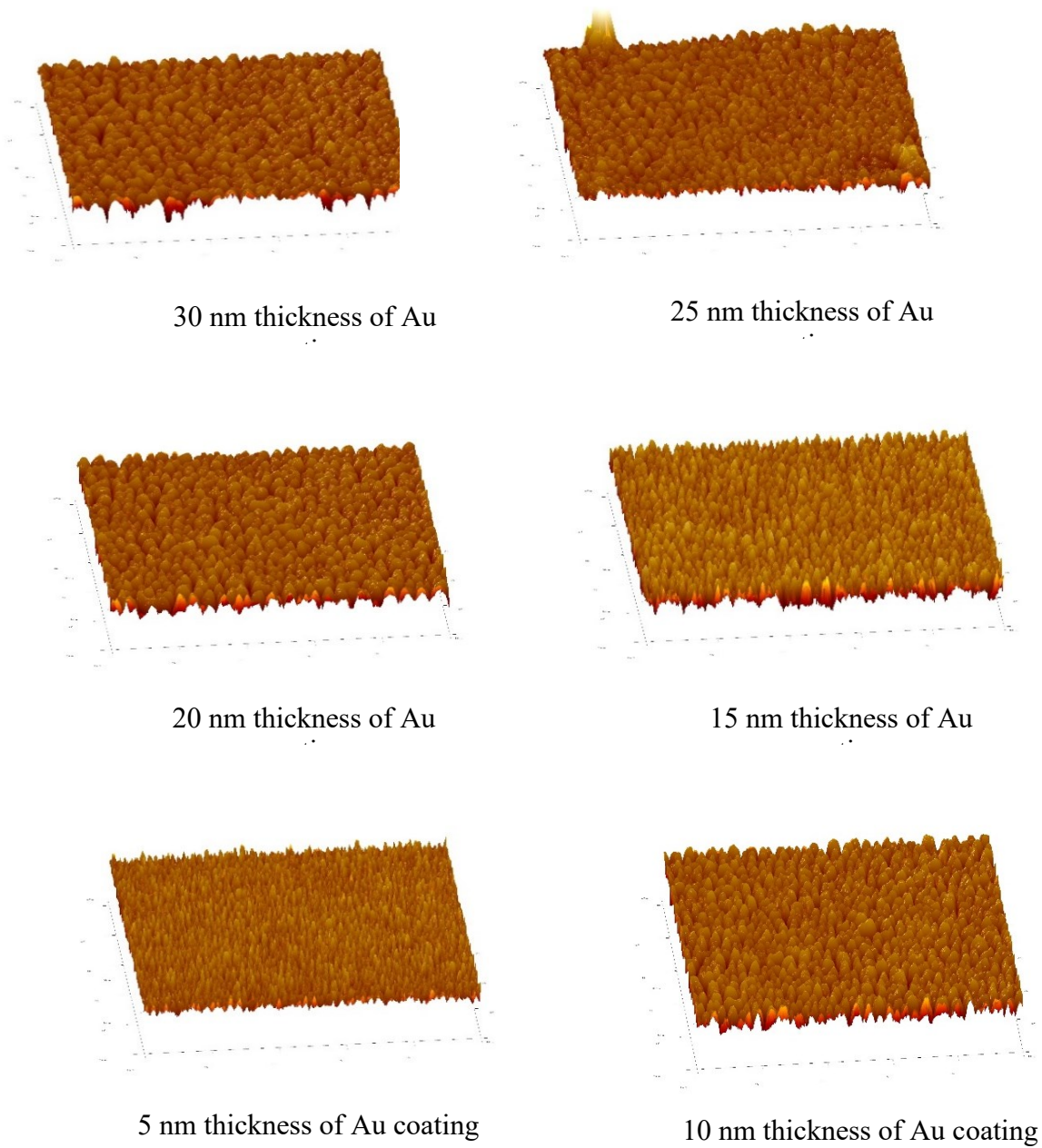
Fig. 5.3. AFM 3-D topographical image of Au coated glass substrates at different coating thickness.

After cleaning and Au deposition, the substrates were biofunctionalized as schematically shown in Fig. 5.4. For this purpose, thiolated DNA strands 5'-GGTTTGGAGGGGC CA-3' were used. An 1 µM DNA solution was prepared with Tris-EDTA buffer at a pH of 7. The DNA solution was kept at 5°C. To biofunctionalize the samples, a 100 µl drop of DNA solution was deposited onto the gold-coated substrates. Next, a 100 µl drop of the MB solution (4.7 mM, Sigma-Aldrich) was added onto the same spot, and the samples were incubated for 24 h at 5°C. The incubation was done in humid environment to avoid drying of the samples. For this purposes, a two-compartment Petri dish was used. The sample was placed in one compartment, and second compartment contained DI water. Fig. 5.5. illustrates the functionalization process.
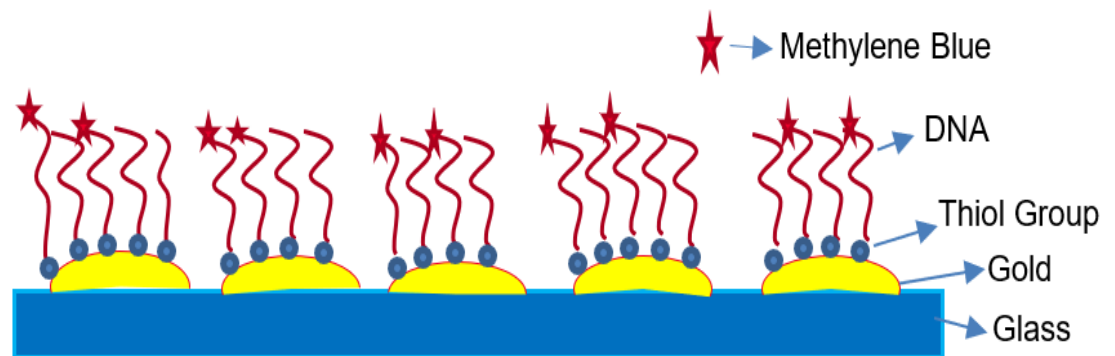
Fig. 5.4. Scheme of DNA functionalized, gold-coated plasmonic substrate.
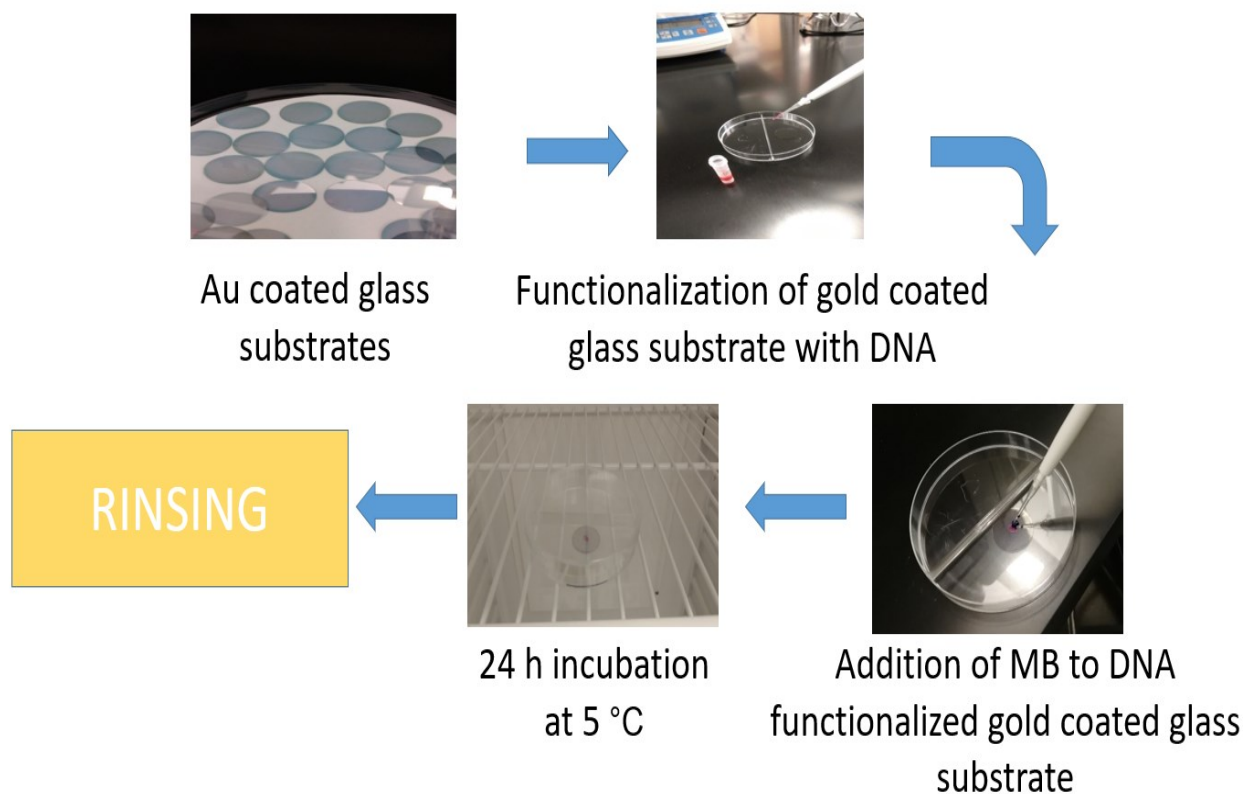
Fig. 5.5. Steps of substrate bio-functionalization with DNA and methylene blue.

It has been expected that during incubation, DNA strands attach to the gold coating through the thiol groups (Pensa et al., 2012), whereas MB binds to guanine bases of DNA(Vardevanyan, Antonyan, Parsadanyan, Shahinyan, & Hambardzumyan, 2013). For comparison, control samples were also prepared by incubating similar gold-coated glass substrates with the MB solution alone in the absence of DNA (Fig.5.4.).

5.2 Benchmark Raman and SERS Characterization of All Components

Fig.5.6 and Fig.5.7. show the benchmark Raman spectra of Tris-EDTA buffer, DNA solution on Gold coated glass substrates. These two are not Raman active, which is evident from their respective Raman spectra.
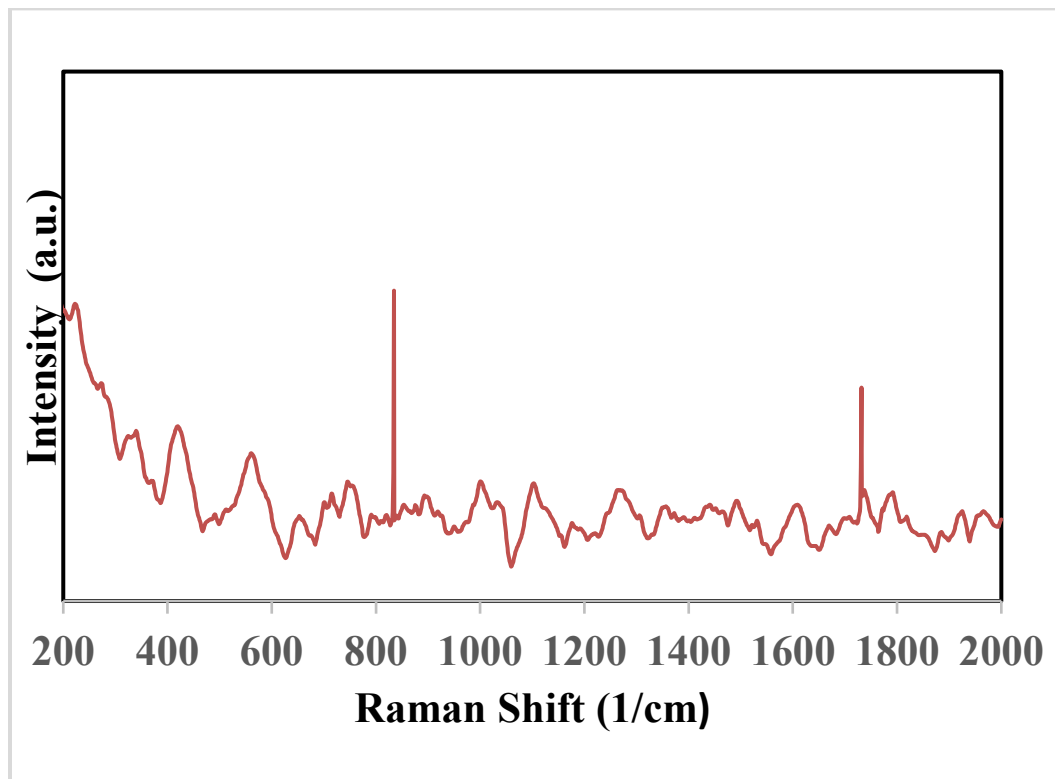
Fig. 5.6. Benchmark Raman spectrum of Tris-EDTA buffer on Au coated glass substrate. No characteristic peaks observed.

Fig. 5.8. Shows a typical benchmark Raman spectrum of methylene blue solution. To prepare this sample, a 100 µL drop of the MB solution was deposited onto a gold-coated glass slide, and Raman characterization was performed immediately without incubation or rinsing. The spectrum exhibits pronounced bands that we have attributed to stretching of C=C bond of MB's aromatic ring at 1625 cm^{-1}; vibrations of C=N bonds

and CH$_3$ groups between 1398 cm^{-1} and 1470 cm^{-1}; and C-N-C skeletal bending at 501 cm^{-1} and 446 cm^{-1} (Nicolai & Rubim, 2003; Xiao & Man, 2007).
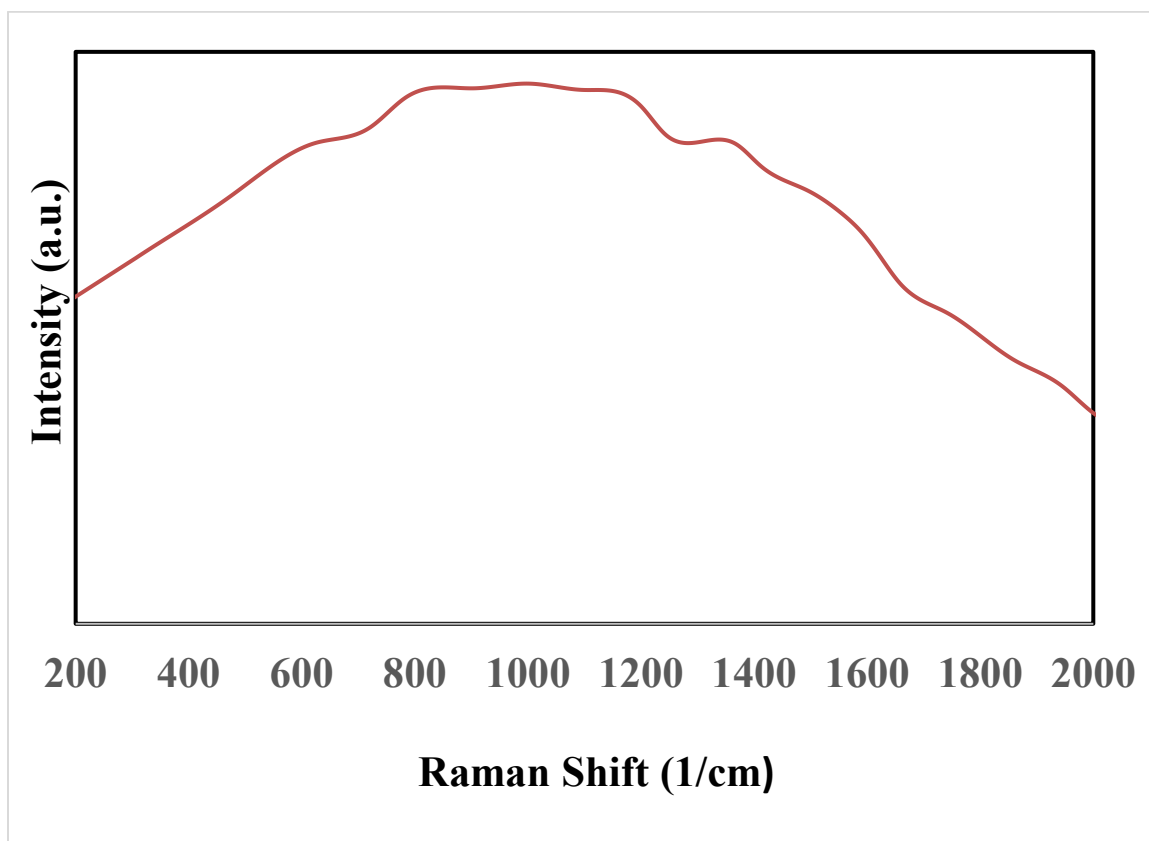
Fig. 5.7. Raman spectrum of ss-DNA incubated on gold coated glass slide.
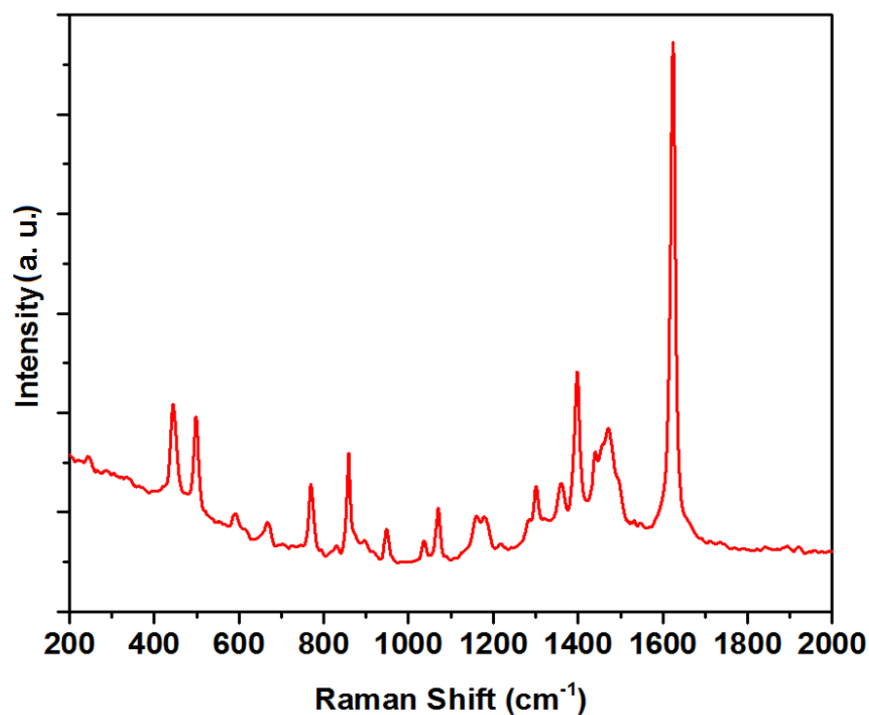
Fig. 5.8. Raman spectrum of methylene blue solution on gold coated glass substrate without incubation

Next, the same amount of MB solution was incubated on gold-coated glass substrates for 24h at 5°C. Then, the samples were rinsed in the Tris-EDTA buffer and their Raman spectra collected. An example spectrum is shown in (Fig. 5.9). It can be seen that in the absence of DNA functionalization, the spectrum does not exhibit Raman bands characteristic of MB. After rinsing the Methylene-Blue gets rinsed off the Au coated glass surface.
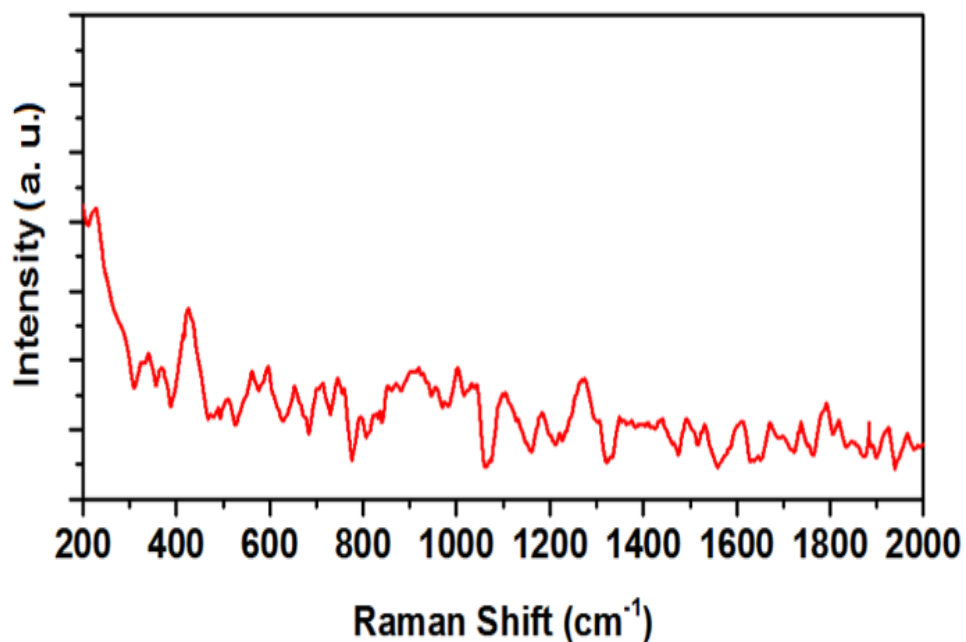
Fig. 5.9. Raman spectrum of rinsed gold-coated glass substrate after a 24 h incubation with methylene blue in the absence of DNA functionalization.

5.3 SERS Detection of Reduction-Oxidation Processes Stimulated by LSPR Hot-Spots under Laser Excitation

Fig. 5.10.shows a SERS spectrum of DNA-functionalized substrate incubated with the addition of MB. In striking contrast with DNA-free experiments., When the Au coated glass substrate is bio-functionalized with the DNA, pronounced Raman bands of methylene blue are visible after rinsing. These include a strong peak at approximately 1623 cm^{-1}.
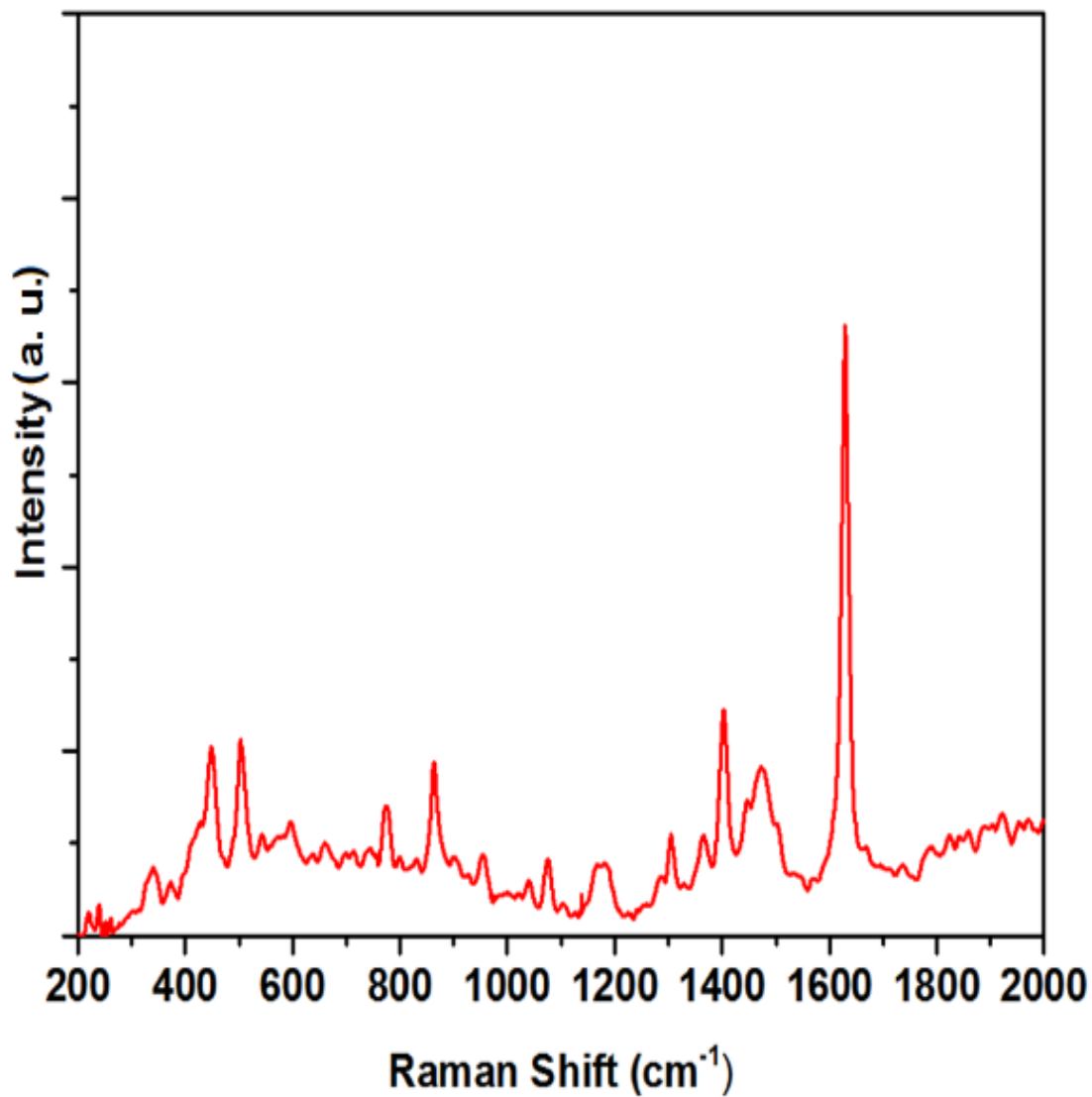
Fig. 5.10. SERS spectrum of DNA-functionalized, MB-loaded gold coated glass substrate after a 24 h incubation and rinsing.

Next, we have investigated the evolution of SERS spectra of DNA-functionalized

and MB-loaded samples after 20 min, 40 min, 60 min, 80 min, 100 min, 120 min, and

140 min of exposure to a 523 nm laser excitation. As it can be seen from Fig 5.11, the Raman bands have decayed with time. After 100 min of exposure to the laser, Raman fingerprint of MB has completely disappeared. Then, we added 20 µL of Tris-EDTA buffer (pH 7) on the same substrate, and continued the laser exposure. Remarkably, this resulted in a recovery of MB's Raman fingerprint. After 160 min, pronounced Raman bands at 1626 cm^{-1} and 1396 cm^{-1} characteristic of MB have been detected again.

Continuing the exposure beyond this point caused the Raman bands disappearing and reappearing again, in a similar reversible fashion. To further investigate this phenomenon we carried out the experiment for a longer period of time and we could see repetitive reduction-oxidation cycles (Fig 5.12.)

For the sake of comparison, we also have deposited a 0.5 µL drop of the MB solution onto a cleaned glass slide without gold coating and DNA functionalization. This control sample was immediately exposed to the 532 nm laser excitation, and the entire experiment was repeated as described above. As Fig. 5.13. illustrates, in this case a characteristic Raman band, centered at approximately 1629 cm^{-1}, has remained after 100 min of exposure. Subsequent addition of 20 µL of Tris-EDTA buffer did not change the Raman fingerprint.
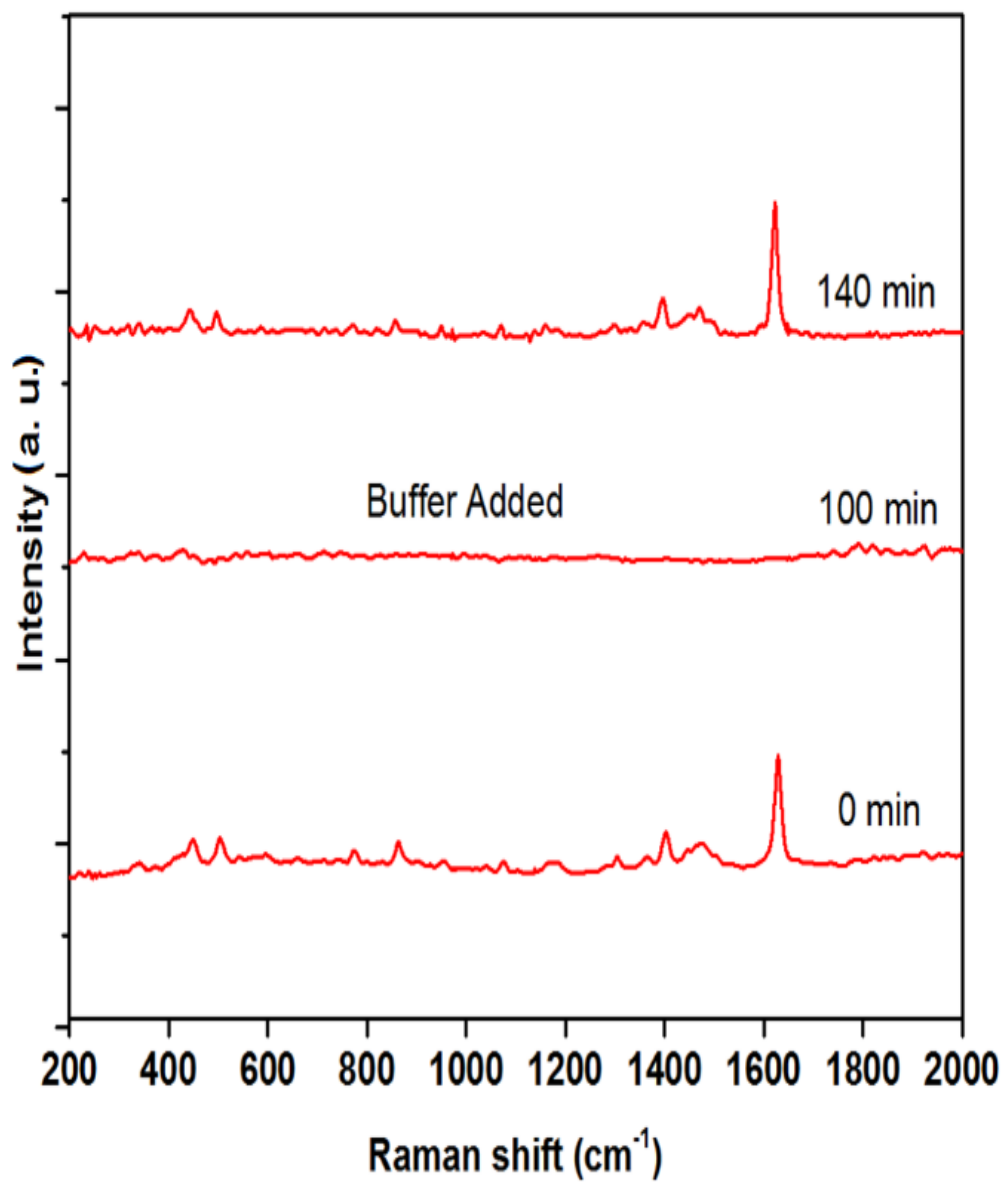
Fig. 5.11. SERS spectra of DNA-functionalized, MB-loaded gold-coated glass substrate at the beginning of a 523 nm laser exposure (bottom); after 100 min of the exposure (middle); and after 140 min of the exposure following the addition of Tris-EDTA buffer (top). A vertical offset was applied to the spectra for clearer presentation.
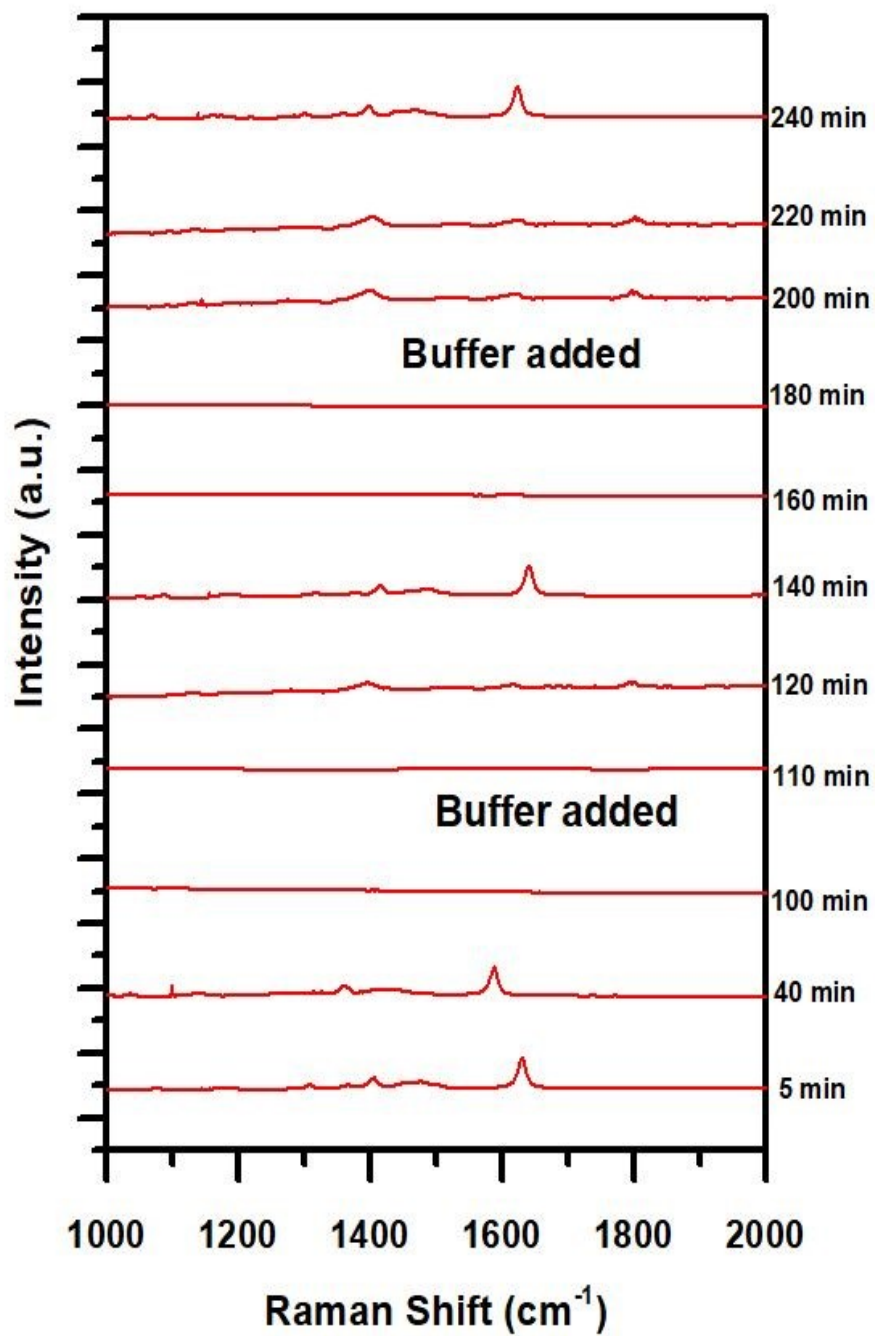
Fig. 5.12. Reduction-oxidation cycle of Methylene blue at neutral pH and in absence of electrode potential on Au coated glass plasmonic substrates.
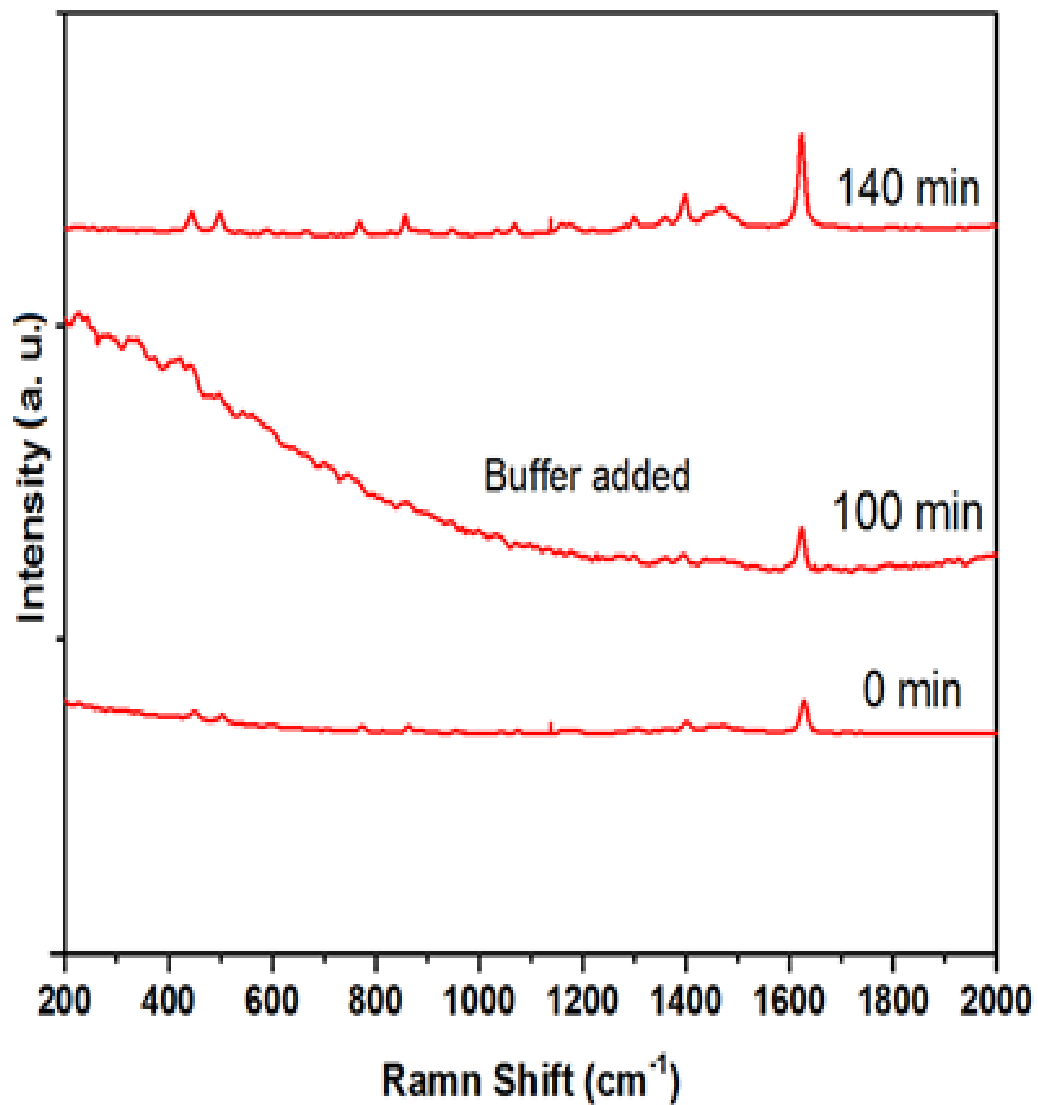
Fig. 5.13. Raman spectra of a drop of MB solution on a bare uncoated glass slide at the beginning of laser exposure (bottom); after 100 min of the exposure (middle); and after 140 min of the exposure following the addition of Tris-EDTA buffer (top). A vertical offset was applied to the spectra for clearer presentation.

CHAPTER SIX : DISCUSSIONS

The results presented in Figs. 5.9 and 5.10 indicate that in the absence of DNA functionalization, methylene blue does not attach to gold-coated substrates strongly enough to remain on the surface after rinsing. However in the presence of DNA, pronounced SERS signal of MB indicates its presence on the surface after rinsing. We expect that during the incubation, DNA binds to the surface of gold through the mediation of thiol groups (Pensa et al., 2012) , whereas MB binds to guanine bases of DNA (Vardevanyan et al., 2013), which plays a role of surface-immobilized linker.

Remarkably, after rinsing of the incubated samples, MB-loaded, surface-immobilized DNA is supposed to be present in a monolayer quantity or less. Therefore, pronounced Raman fingerprints such as shown in Fig. 5.10 correspond to a very small quantity of MB molecules, indicating significant SERS enhancement in our samples.

A well-known redox indicator, MB can adopt oxidized or reduced forms, which differ in charge and protonation state(Farjami, Clima, Gothelf, & Ferapontova, 2010). In water or buffer solution at neutral or acidic pH conditions MB would adopt an oxidized form, which produces a characteristic Raman spectrum such as shown in Fig. 5.8. As our results indicate, similar fingerprints are also observed in SERS spectra from MB-loaded, substrate-immobilized DNA after relatively short exposures to laser excitation (Figs. 5.10, 5.11 and 5.12). However, more extensive exposures to the laser light in the presence of the buffer have resulted in disappearance of the Raman fingerprint (Fig.5.11).

Degradation of Raman bands of MB can be attributed to its reduction, as it was demonstrated by electrochemical stimulation of DNA-bound MB (Papadopoulou et al., 2016). In this published work (Papadopoulou et al., 2016), double stranded DNA loaded

with methylene blue was immobilized on gold electrodes. Incubated overnight and MB pigments were immobilized after the incubation. The changed electrode potential was changed from 0 mV to -500 mV at a rate of 0.7mV/s. This resulted in a gradual decrease of the Raman bands with the applied potential (Fig. 5.14(a)). In particular, the peaks at 1622 cm^{-1} and 1388 cm^{-1} which correspond to the aromatic C=C and C=N ring stretches, have decreased with height and eventually disappeared completely at ~ -500mV. When the potential is reversed from -500mV to 0mV, the Raman peaks reappeared. (Fig. 5.14 (b)). Based on these results, disappearance of MB's characteristic Raman bands can be indicative of its reduction, and vice versa.

Therefore, we expect that the changes of Raman Spectra that we observe indicate reduction of MB, followed by oxidation. Importantly, in our work, the observed reversible reduction-oxidation transformations of MB occurred at neutral pH in the absence of electrodes or chemical agents other than the buffer. However, the presence of gold coating has been critical for these transformations. As Fig. 5.13 indicates, exposure to laser excitation did not induce a reduction of MB solution on a bare un-coated glass slide. From 5.12. we conclude that this reversible reduction-oxidation cycle can be repetitive during prolonged laser exposure and with the addition of buffer solution. We hypothesize that energy of plasmonic hot-spots generated by laser excitation in the gold coating is required for the reversible transformation of MB to occur.
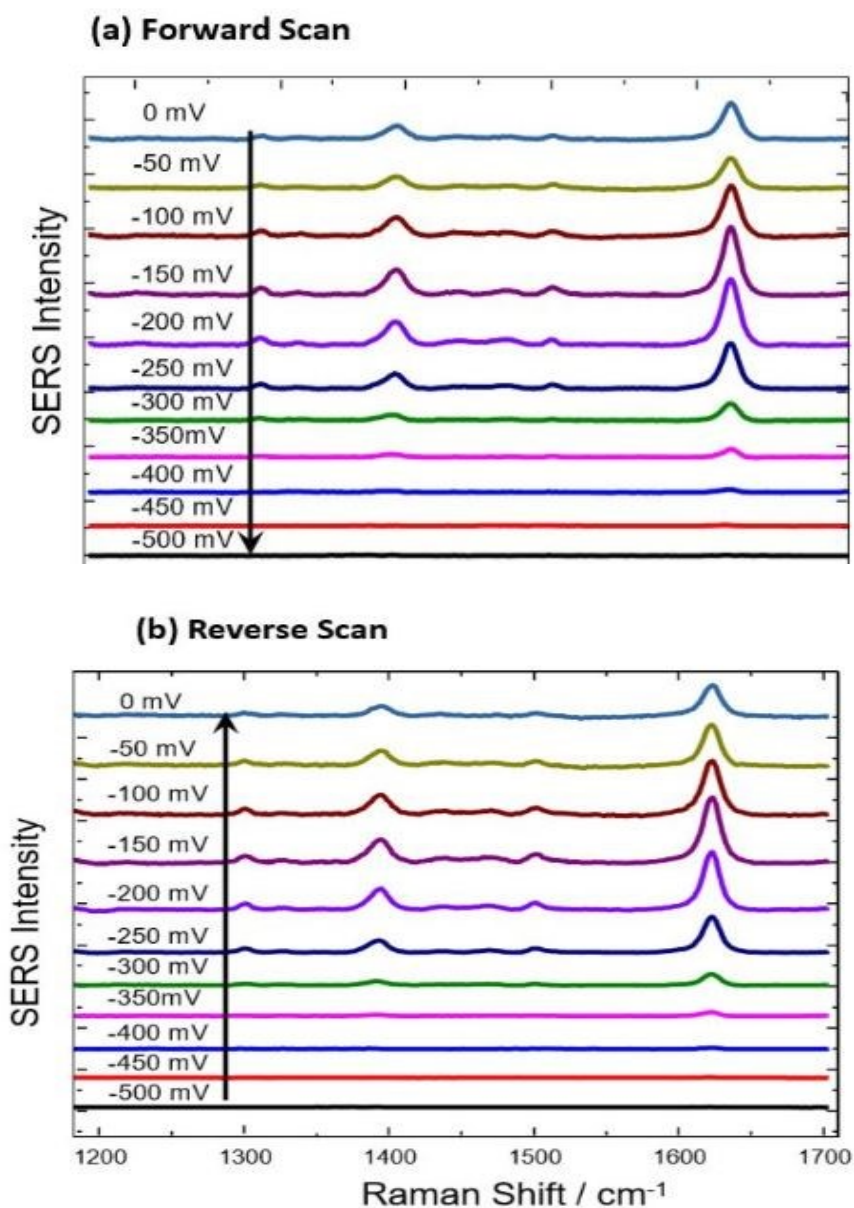
Fig. 5.14. Raman spectra demonstrating electrochemically-driven reduction-oxidation of MB. Reduction of MB : (a) With increasing negative electrode potential, the characteristic peaks of MB dies down and disappears at ~ - 500 m V. Oxidation of MB: (b) When the potential is reversed the characteristic peaks starts reappearing. Reproduced with permission from Ref (Papadopoulou et al., 2016)- Published by The Royal Society of Chemistry.

CHAPTER SEVEN: CONCLUSIONS

In this work, multi-functional application of nanopalsmonics has been demonstrated. This includes inducing chemical changes into a material immobilized on a plasmonic substrate, and detection of these changes using SERS within the same experimental platform. In particular:

- Plasmonic substrates comprising gold nanostructures on glass were fabricated and characterized;

- A process of functionalization of the substrates by DNA carrying an important reduction-oxidation indicator methylene blue, was developed;

- Immobilized, DNA-bound MB was detected by SERS in submonolayer quantities;

- Reduction-oxidation of MB at neutral pH was detected in the same design;

- These chemical changes are attributable to the influence of plasmonic 'hot-spots' under laser excitation in the presence of the buffer.

The results of this research can be useful for many other systems, in particular, this research work has paved the way to the further investigation of plasmonic photocatalysis. Future research may include:

1. Theoratical study of the reversible reduction-oxidation of MB in this system at neutral pH.

2. Development of bio functionalization processes of plasmonic substrates to immobilize different materials.

3. Building models that can simulate plasmonic photocatalysis in various designs.

REFERENCES

Anker, J. N., Hall, W. P., Lyandres, O., Shah, N. C., Zhao, J., & Van Duyne, R. P. (2008a). Biosensing with plasmonic nanosensors. *Nature Materials*, *7*(6), 442–453. https://doi.org/10.1038/nmat2162

Anker, J. N., Hall, W. P., Lyandres, O., Shah, N. C., Zhao, J., & Van Duyne, R. P. (2008b). Biosensing with plasmonic nanosensors. *Nature Materials*, *7*(6), 442–453. https://doi.org/10.1038/nmat2162

Atwater, H. A., & Polman, A. (2010). Plasmonics for improved photovoltaic devices. *Nature Materials*, *9*(3), 205–213. https://doi.org/10.1038/nmat2629

Bantz, K. C., Meyer, A. F., Wittenberg, N. J., Im, H., Kurtuluş, O., Lee, S. H., … Haynes, C. L. (2011a). Recent progress in SERS biosensing. *Physical Chemistry Chemical Physics : PCCP*, *13*(24), 11551–11567. https://doi.org/10.1039/c0cp01841d

Bantz, K. C., Meyer, A. F., Wittenberg, N. J., Im, H., Kurtuluş, Ö., Lee, S. H., … Haynes, C. L. (2011b). Recent progress in SERS biosensing. *Physical Chemistry Chemical Physics*, *13*(24), 11551. https://doi.org/10.1039/c0cp01841d

Barnes, W. L., Dereux, A., & Ebbesen, T. W. (2003). Surface plasmon subwavelength optics. *Nature*, *424*(6950), 824–830. https://doi.org/10.1038/nature01937

Brosseau, C. L., Casadio, F., & Van Duyne, R. P. (2011). Revealing the invisible: using surface-enhanced Raman spectroscopy to identify minute remnants of color in Winslow Homer's colorless skies. *Journal of Raman Spectroscopy*, *42*(6), 1305–1310. https://doi.org/10.1002/jrs.2877

Cao, Y. C., Jin, R., & Mirkin, C. A. (2002a). Nanoparticles with Raman spectroscopic fingerprints for DNA and RNA detection. *Science (New York, N.Y.)*, *297*(5586), 1536–1540. https://doi.org/10.1126/science.297.5586.1536

Cao, Y. C., Jin, R., & Mirkin, C. A. (2002b). Nanoparticles with Raman Spectroscopic Fingerprints for DNA and RNA Detection. *Science*, *297*(5586), 1536 LP-1540. Retrieved from http://science.sciencemag.org/content/297/5586/1536.abstract

Chen, X., Zhu, H., Zhao, J., Zheng, Z., & Gao, X. (2008). Visible-Light-Driven Oxidation of Organic Contaminants in Air with Gold Nanoparticle Catalysts on Oxide Supports. *Angewandte Chemie International Edition*, *47*(29), 5353–5356. https://doi.org/10.1002/anie.200800602

Cheng, J. Y., Mayes, A. M., & Ross, C. A. (2004). Nanostructure engineering by

templated self-assembly of block copolymers. *Nature Materials*, *3*(11), 823–828. https://doi.org/10.1038/nmat1211

Dew, S. K., & Stepanova, M. (2012). Directions in Nanofabrication. In *Nanofabrication* (pp. 3–8). Vienna: Springer Vienna. https://doi.org/10.1007/978-3-7091-0424-8_1

Dey, S., & Zhao, J. (2016). Plasmonic Effect on Exciton and Multiexciton Emission of Single Quantum Dots. *The Journal of Physical Chemistry Letters*, *7*(15), 2921–2929. https://doi.org/10.1021/acs.jpclett.6b01164

Dieringer, J. A., McFarland, A. D., Shah, N. C., Stuart, D. A., Whitney, A. V, Yonzon, C. R., … Van Duyne, R. P. (2006). Surface enhanced Raman spectroscopy: new materials, concepts, characterization tools, and applications. *Faraday Discussions*, *132*, 9–26. Retrieved from http://www.ncbi.nlm.nih.gov/pubmed/16833104

Doktycz, S. J., & Suslick, K. S. (1990). Interparticle collisions driven by ultrasound. *Science (New York, N.Y.)*, *247*(4946), 1067–1069. https://doi.org/10.1126/science.2309118

Farjami, E., Clima, L., Gothelf, K. V., & Ferapontova, E. E. (2010). DNA interactions with a Methylene Blue redox indicator depend on the DNA length and are sequence specific. *The Analyst*, *135*(6), 1443. https://doi.org/10.1039/c0an00049c

Giljohann, D. A., Seferos, D. S., Daniel, W. L., Massich, M. D., Patel, P. C., & Mirkin, C. A. (2010). Gold Nanoparticles for Biology and Medicine. *Angewandte Chemie International Edition*, *49*(19), 3280–3294. https://doi.org/10.1002/anie.200904359

Haynes, C. L., McFarland, A. D., & Duyne, R. P. Van. (2005). Surface-Enhanced Raman Spectroscopy. *Analytical Chemistry*, *77*(17), 338 A-346 A. https://doi.org/10.1021/ac053456d

Homola, J., Yee, S. S., & Gauglitz, G. (1999). Surface plasmon resonance sensors: review. *Sensors and Actuators B: Chemical*, *54*(1–2), 3–15. https://doi.org/10.1016/S0925-4005(98)00321-9

Jalili, N., & Laxminarayana, K. (2004). A review of atomic force microscopy imaging systems: application to molecular metrology and biological sciences. *Mechatronics*, *14*(8), 907–945. https://doi.org/10.1016/J.MECHATRONICS.2004.04.005

Kelly, P. ., & Arnell, R. . (2000). Magnetron sputtering: a review of recent developments and applications. *Vacuum*, *56*(3), 159–172. https://doi.org/10.1016/S0042-207X(99)00189-X

Kim, S. M., Lee, S. W., Moon, S. Y., & Park, J. Y. (2016a). The effect of hot electrons and surface plasmons on heterogeneous catalysis. *Journal of Physics: Condensed Matter*, *28*(25), 254002. https://doi.org/10.1088/0953-8984/28/25/254002

Kim, S. M., Lee, S. W., Moon, S. Y., & Park, J. Y. (2016b). The effect of hot electrons and surface plasmons on heterogeneous catalysis. *Journal of Physics: Condensed Matter*, *28*(25), 254002. https://doi.org/10.1088/0953-8984/28/25/254002

Knight, D. S., & White, W. B. (1989). Characterization of diamond films by Raman spectroscopy. *Journal of Materials Research*, *4*(02), 385–393. https://doi.org/10.1557/JMR.1989.0385

Kulkarni, A. P., Noone, K. M., Munechika, K., Guyer, S. R., & Ginger, D. S. (2010). Plasmon-Enhanced Charge Carrier Generation in Organic Photovoltaic Films Using Silver Nanoprisms. *Nano Letters*, *10*(4), 1501–1505. https://doi.org/10.1021/nl100615e

Lal, S., Grady, N. K., Kundu, J., Levin, C. S., Lassiter, J. B., & Halas, N. J. (2008). Tailoring plasmonic substrates for surface enhanced spectroscopies. *Chemical Society Reviews*, *37*(5), 898. https://doi.org/10.1039/b705969h

Li, T., Wu, X., Tao, G., Yin, H., Zhang, J., Liu, F., & Li, N. (2018). A simple and non-amplification platform for femtomolar DNA and microRNA detection by combining automatic gold nanoparticle enumeration with target-induced strand-displacement. *Biosensors and Bioelectronics*, *105*, 137–142. https://doi.org/10.1016/j.bios.2018.01.034

Liu, D., Yang, D., Gao, Y., Ma, J., Long, R., Wang, C., & Xiong, Y. (2016). Flexible Near-Infrared Photovoltaic Devices Based on Plasmonic Hot-Electron Injection into Silicon Nanowire Arrays. *Angewandte Chemie*, *128*(14), 4653–4657. https://doi.org/10.1002/ange.201600279

Liu, H., Zhang, L., Lang, X., Yamaguchi, Y., Iwasaki, H., Inouye, Y., … Chen, M. (2011). Single molecule detection from a large-scale SERS-active Au79Ag21 substrate. *Scientific Reports*, *1*(1), 112. https://doi.org/10.1038/srep00112

Meyer, E. (1992). Atomic force microscopy. *Progress in Surface Science*, *41*(1), 3–49. https://doi.org/10.1016/0079-6816(92)90009-7

Mirkin, C. A., Letsinger, R. L., Mucic, R. C., & Storhoff, J. J. (1996). A DNA-based method for rationally assembling nanoparticles into macroscopic materials. *Nature*, *382*(6592), 607–609. https://doi.org/10.1038/382607a0

Mohammad, M. A., Muhammad, M., Dew, S. K., & Stepanova, M. (2012). Fundamentals of Electron Beam Exposure and Development. In *Nanofabrication* (pp. 11–41). Vienna: Springer Vienna. https://doi.org/10.1007/978-3-7091-0424-8_2

Naldoni, A., Riboni, F., Guler, U., Boltasseva, A., Shalaev, V. M., & Kildishev, A. V. (2016). Solar-Powered Plasmon-Enhanced Heterogeneous Catalysis. *Nanophotonics*, *5*(1), 112–133. https://doi.org/10.1515/nanoph-2016-0018

Nicolai, S. H. A., & Rubim, J. C. (2003). Surface-Enhanced Resonance Raman (SERR) Spectra of Methylene Blue Adsorbed on a Silver Electrode. *Langmuir*, *19*(10), 4291–4294. https://doi.org/10.1021/la034076v

Oakley, L. H., Dinehart, S. A., Svoboda, S. A., & Wustholz, K. L. (2011). Identification of Organic Materials in Historic Oil Paintings Using Correlated Extractionless Surface-Enhanced Raman Scattering and Fluorescence Microscopy. *Analytical Chemistry*, *83*(11), 3986–3989. https://doi.org/10.1021/ac200698q

Papadopoulou, E., Gale, N., Thompson, J. F., Fleming, T. A., Brown, T., & Bartlett, P. N. (2016). Specifically horizontally tethered DNA probes on Au surfaces allow labelled and label-free DNA detection using SERS and electrochemically driven melting. *Chemical Science*, *7*(1), 386–393. https://doi.org/10.1039/C5SC03185K

Paxton, W. F., Kleinman, S. L., Basuray, A. N., Stoddart, J. F., & Van Duyne, R. P. (2011). Surface-Enhanced Raman Spectroelectrochemistry of TTF-Modified Self-Assembled Monolayers. *The Journal of Physical Chemistry Letters*, *2*(10), 1145–1149. https://doi.org/10.1021/jz200523q

Pensa, E., Cortés, E., Corthey, G., Carro, P., Vericat, C., Fonticelli, M. H., … Salvarezza, R. C. (2012). The Chemistry of the Sulfur–Gold Interface: In Search of a Unified Model. *Accounts of Chemical Research*, *45*(8), 1183–1192. https://doi.org/10.1021/ar200260p

Persson, B. N. J., & Ryberg, R. (1981). Vibrational interaction between molecules adsorbed on a metal surface: The dipole-dipole interaction. *Physical Review B*, *24*(12), 6954–6970. https://doi.org/10.1103/PhysRevB.24.6954

Peters, R. F., Gutierrez-Rivera, L., Dew, S. K., & Stepanova, M. (2015). Surface Enhanced Raman Spectroscopy Detection of Biomolecules Using EBL Fabricated Nanostructured Substrates. *Journal of Visualized Experiments*, (97), e52712–e52712. https://doi.org/10.3791/52712

Raman, C. V., & Krishnan, K. S. (1928). A New Type of Secondary Radiation. *Nature*, *121*(3048), 501–502. https://doi.org/10.1038/121501c0

Ravindran, A., Chandran, P., & Khan, S. S. (2013). Biofunctionalized silver nanoparticles: Advances and prospects. *Colloids and Surfaces B: Biointerfaces*, *105*, 342–352. https://doi.org/10.1016/j.colsurfb.2012.07.036

Roh, J. Y., Matecki, M. K., Svoboda, S. A., & Wustholz, K. L. (2016). Identifying Pigment Mixtures in Art Using SERS: A Treatment Flowchart Approach. *Analytical Chemistry*, *88*(4), 2028–2032. https://doi.org/10.1021/acs.analchem.6b00044

Sharma, B., Frontiera, R. R., Henry, A.-I., Ringe, E., & Van Duyne, R. P. (2012). SERS: Materials, applications, and the future. *Materials Today*, *15*(1–2), 16–25.

https://doi.org/10.1016/S1369-7021(12)70017-2

Sylvia, J. M., Janni, J. A., Klein, J. D., & Spencer, K. M. (2000). Surface-Enhanced Raman Detection of 2,4-Dinitrotoluene Impurity Vapor as a Marker To Locate Landmines. *Analytical Chemistry*, *72*(23), 5834–5840. https://doi.org/10.1021/ac0006573

Thornton, J. A. (1978). Magnetron sputtering: basic physics and application to cylindrical magnetrons. *Journal of Vacuum Science and Technology*, *15*(2), 171–177. https://doi.org/10.1116/1.569448

Vardevanyan, P. O., Antonyan, A. P., Parsadanyan, M. A., Shahinyan, M. A., & Hambardzumyan, L. A. (2013). Mechanisms for Binding between Methylene Blue and DNA. *Journal of Applied Spectroscopy*, *80*(4), 595–599. https://doi.org/10.1007/s10812-013-9811-7

Weitz, D. A., Garoff, S., Gersten, J. I., & Nitzan, A. (1983). The enhancement of Raman scattering, resonance Raman scattering, and fluorescence from molecules adsorbed on a rough silver surface. *The Journal of Chemical Physics*, *78*(9), 5324–5338. https://doi.org/10.1063/1.445486

Wu, K., Chen, J., McBride, J. R., & Lian, T. (2015). Efficient hot-electron transfer by a plasmon-induced interfacial charge-transfer transition. *Science*, *349*(6248), 632–635. https://doi.org/10.1126/science.aac5443

Xiao, G.-N., & Man, S.-Q. (2007). Surface-enhanced Raman scattering of methylene blue adsorbed on cap-shaped silver nanoparticles. *Chemical Physics Letters*, *447*(4–6), 305–309. https://doi.org/10.1016/J.CPLETT.2007.09.045

Xie, W., & Schlücker, S. (2014). Rationally designed multifunctional plasmonic nanostructures for surface-enhanced Raman spectroscopy: a review. *Reports on Progress in Physics*, *77*(11), 116502. https://doi.org/10.1088/0034-4885/77/11/116502

Yagi, N., Satonaka, K., Horio, M., Shimogaki, H., Tokuda, Y., & Maeda, S. (1996). The Role of DNase and EDTA on DNA Degradation in Formaldehyde Fixed Tissues. *Biotechnic & Histochemistry*, *71*(3), 123–129. https://doi.org/10.3109/10520299609117148

Ye, W., Long, R., Huang, H., & Xiong, Y. (2017). Plasmonic nanostructures in solar energy conversion. *Journal of Materials Chemistry C*, *5*(5), 1008–1021. https://doi.org/10.1039/C6TC04847A

Zeng, Z., Liu, Y., & Wei, J. (2016). Recent advances in surface-enhanced raman spectroscopy (SERS): Finite-difference time-domain (FDTD) method for SERS and sensing applications. *TrAC Trends in Analytical Chemistry*, *75*, 162–173.